Golgi apposition promotes the generation of specialized lysosomes in differentiated keratinocytes

Sarmistha Mahanty[1*], Ptissam Bergam[2], Vivek Belapurkar[3], Litralson Eluvathingal[3], Nikita Gupta[1], Deepak Nair[3], Graca Raposo[2#], Subba Rao Gangi Setty[1*#]

[1]Department of Microbiology and Cell Biology, Indian Institute of Science, Bangalore 560012 India; [2]Institut Curie, PSL Research University, CNRS, UMR 144, Structure and Membrane Compartments, F-75005, Paris, France, [3]Centre for Neuroscience, Indian Institute of Science, Bangalore 560012 India

Corresponding authors:
[*]Sarmistha Mahanty - sarmistham@iisc.ac.in
[*]Subba Rao Gangi Setty – subba@iisc.ac.in

Foot notes:
# Authors contributed equally to this work
Lead contact: subba@iisc.ac.in

Phone: +91-80-22932297
Fax: +91-80-23602697

Running title: Lysosome function requires Golgi apposition

Key points:
- Calcium-induced differentiation of human keratinocytes results in the dispersal of functional Golgi stacks and lysosomes
- Dispersed Golgi stacks remain in close apposition with the lysosomes.
- Golgi tether GRASP65 surrounds keratinocyte lysosomes
- GRASP65 depletion disrupts Golgi-lysosome apposition and results in malfunctional lysosomes
- Lysosomes of differentiated keratinocytes generate from *trans*-Golgi

Key words: Differentiation, Golgi, GRASP65, Golgi derived lysosomes, Golgi-lysosome contact, keratinocytes

Abstract
Lysosomes, the major degradative compartments of the cell acquire unique properties upon receiving external signals. In the skin, epidermal keratinocytes follow a gradual differentiation process from the basal to the upper skin layers with consequent changes in cellular morphology and intracellular organelles. Previous studies show that keratinocyte differentiation relies on increased lysosome biogenesis. However, the mechanisms of the generation and maintenance of keratinocyte lysosomes remain unknown. Here, we show that dispersed Golgi stacks are distributed to the proximity of lysosomes in differentiated keratinocytes, facilitated by the Golgi tethering protein GRASP65 which associates with the lysosomes. Inhibition of GRASP65 results in the loss of Golgi-lysosome apposition. Further studies exploiting small molecule inhibition and gene modulation reveal a direct role of functional Golgi and its apposition in the generation and, maturation of keratinocyte lysosomes. Selective accumulation of secretory cargo and *trans*-Golgi enzyme in the lysosome lumen and, reversible dissociation in presence of brefeldin A or Golgicide-A suggests Golgi origin of keratinocyte lysosomes. Taken together, unique Golgi -lysosome apposition and the unconventional properties of keratinocyte lysosomes indicate their possible distinct roles in epidermis homeostasis.

Introduction
Although compartmentalized as mini systems, intracellular organelles do communicate in form of physical proximity or contact, to maintain cellular homeostasis. This close apposition of 20 - 40 nm facilitates the exchange of materials for example signaling molecules, lipids etc. between organelles (Bravo-Sagua et al., 2014). Lysosomes are highly dynamic intracellular organelles that perform diverse cellular functions and respond to extra/intracellular changes toward homeostasis (reviewed in (Ballabio and Bonifacino, 2020). In line, lysosome function is also supported by its contact with other organelles such as mitochondria, ER, and peroxisome (Atakpa et al., 2018; Chu et al., 2015; Wong et al., 2019). Conventionally, lysosomes are formed by the sequential maturation of early endosomes upon receiving lysosomal hydrolases and membrane proteins from the Golgi through tubulo-vesicular carriers (Kornfeld and Mellman, 1989; Krause, 2000; Murphy, 1991). On the other hand, several secretory organelles such as Weibel-Palade bodies (WPBs) and neuronal secretory granules (a set of lysosome-related organelles, LROs) originate from the Golgi followed by sequential maturation through endocytic input (Delevoye et al., 2019). However, physical contact between lysosomes/late endocytic organelles with Golgi has not yet been reported. This is possibly due to the compact Golgi morphology that limits the availability of Golgi beyond the perinuclear region (reviewed in (David et al., 2021).

Golgi in mammalian cells is a perinuclearly localized compact structure consisting of multiple cisternae. The latter is arranged in form of a ribbon that favors a complex glycosylation process (Xiang and Wang, 2010; Xiang et al., 2013). Golgi disassembles to meet higher secretory demand in certain physiological conditions and, in mitosis which facilitates the segregation between daughter cells followed by reassembly (Ayala et al., 2020). For instance, Golgi dispersion occurs in neurons during high neuronal activity, in prolactin cells of female rats induced by sucking stimulus, Brunner's gland cells in platypus and, during cellular differentiation (Krause, 2000; Rambourg et al., 1993; Thayer et al., 2013; Wei and Seemann, 2017). The dynamic morphology and function of Golgi are regulated by Golgi-associated structural and functional proteins namely Golgi reassembly stacking proteins (GRASP55, GRASP65), and ADP-ribosylation factor1 (Arf1) (Donaldson et al., 2005; Satoh et al., 2015). GRASP55 and GRASP65 play essential and complementary functions in maintaining Golgi ribbon morphology (Xiang and Wang, 2010). These proteins

link the Golgi stacks through oligomerization regulated by several GTPases like CDKs and polo-like kinases (Wang et al., 2005; Xiang and Wang, 2010; Zhang and Wang, 2015). The small GTPase Arf1 regulates intra-Golgi and Golgi-ER transport by the generation of COPI (coat protein I complex) vesicles (Donaldson et al., 2005; Spang, 2002). It is established that higher secretion requires the generation of more COPI vesicles, and the latter is positively regulated by the dispersion of Golgi stacks. Accordingly, Golgi dispersion due to the knockdown of GRASP55 or GRASP65 leads to the generation of more COPI vesicles in an *in vitro* budding assay (Wang et al., 2008).

Recent studies established molecular overlap between Golgi and lysosome. For example, lysosome localized kinase mTORC1 also localizes with the Golgi membrane and is activated through Golgi localized small GTPase Rab1 and, Golgi membrane tether GOLPH3 (reviewed in (Makhoul and Gleeson, 2021; Scott et al., 2009; Thomas et al., 2014). Furthermore, the perinuclear localization of lysosomes during starvation is influenced by the interaction between Golgi small GTPase Rab34 and lysosome-localized RILP, an effector of the tumor suppressor protein FLCN (Starling et al., 2016; Wang and Hong, 2002). Direct physical contact of Golgi peripheral protein GRASP55 with LC3II and LAMP2 has been shown to facilitate unconventional secretion from autophagosomes during starvation (Zhang and Wang, 2018). Additionally, the generation and maturation of presynaptic precursors require cross-talk between the small GTPases Rab2 and Arl8B, localized to Golgi and lysosomes respectively (Gotz et al., 2021). Post-Golgi transport carriers are shown to shuttle lysosomal components in the axon bidirectionally and confer lysosomal characteristics (Lie et al., 2021). However, direct physical contact between Golgi and lysosomes is not yet established.

In this study, we show that lysosomes of differentiated keratinocytes remain organized in close proximity to the dispersed Golgi stacks which facilitates receiving of Golgi input, required for lysosome maturation. This close apposition between Golgi and lysosome is mediated by the Golgi tethering proteinGRASP65 (but not GRASP55) which associates with the lysosome membrane in differentiated keratinocytes. Selective accumulation of secretary Golgi cargo and a *trans*-Golgi enzyme galT in the lumen suggest keratinocyte lysosomes as modified *trans*-Golgi derived vesicular carriers. Therefore, this study unravels the existence of Golgi-lysosome cross talk and emphasize its significance in the generation of specialized lysosomes in differentiated keratinocytes. A similar inter organelle cross talk may exist in other secretory cell types.

Results

Lysosomes of control and differentiated keratinocytes possess similar conventional characteristics

We demonstrated increased lysosome biogenesis during calcium-induced differentiation of human primary keratinocytes (Mahanty et al., 2019). Here, we attempt a comparative analysis of the lysosomes of proliferative (referred to here as ‘Control’) and differentiated keratinocytes (referred to here as 'Differentiated’ or ‘Diff.’) by immunofluorescence microscopy (IFM). IFM analysis of LAMP1 (a marker of lysosomes) revealed an extensive peripheral distribution of lysosomes in the differentiated cell cytoplasm compared to their perinuclear localization in control cells (Fig. 1A) (Mahanty et al., 2019). In addition, the average number of lysosomes/μm^2 area and, the average size (in μm^2) of the lysosomes were significantly high in differentiated compared to the control keratinocytes (Fig. 1B; mean difference = 0.13±0.01 and, Fig. 1C; mean difference = 0.21±0.01). Visually, the lysosomes of differentiated keratinocytes appeared in two different morphologies: bright, filled/solid structures (denoted here as ‘A’ type), and comparatively less intense big doughnut-shaped

structures (denoted here as ‘B’ type) (zoomed inset of Differentiated, Fig. 1A). Accordingly, LAMP1 intensity of ‘A’ type was significantly higher in compared to the ‘B’ type lysosomes of differentiated keratinocytes (Fig. 1D). In addition to the A and B types, a population of very small LAMP1 structures that possibly represent the LAMP1 carriers (Pols et al., 2013) were also present (white arrowheads in Fig. 1A). We had a similar observation in time series experiments wherein small LAMP1 carriers (LAMP1-RFP) showed assembly/fusion with the lysosomes (arrowheads in Fig. S1A, Video S1). In contrast, the lysosome population of the control keratinocytes represent solid and bright LAMP1 structures that likely to correlate to the ‘A’ type in differentiated cells. To note, the entire population of LAMP1-positive lysosomes in control and differentiated keratinocytes was also positive for lysosomal membrane proteins CD63 and LAMP2 (Figs. 1E and S1B).

Based on apparent morphological differences, we hypothesized differential functional characteristics of the lysosomes in control and differentiated keratinocytes. To that end, lysosomes were further analyzed on the basis of the presence of hydrolase cathepsin D, which marks the active lysosomes (Bright et al., 2016) and, the uptake of soluble cargoes for example LysoTracker Red DND99 and dextran-fluorescein. Coimmunostaining experiments revealed that the majority of the LAMP1-positive lysosomes were positive for cathepsin D in both control and differentiated cells (Fig. 1F, arrowheads). This result was further corroborated by the uptake of cathepsin B substrate magic red to these lysosomes (data not shown). LysoTracker Red (LR) is a membrane permeable weak base which is used as acidotropic probe to mark acidic compartments of the cell. Uptake of LR followed by LAMP1 immunostaining revealed that the majority of the lysosome population was also positive for LR both in control and differentiated keratinocytes (Fig. S1C). However, a small population of cathepsin D-negative, LR-negative small LAMP1 structures was also present in differentiated keratinocytes (white stars in Fig.1F and Fig. S1C). On the other hand, perinuclear localized structures of control keratinocytes were positive for cathepsin D and LR except for a small lysosome pool in the outer perinuclear region (Fig. S1C). We hypothesize that the population of cathepsin D-negative and LR-negative LAMP1-positive lysosomes may represent the inactive lysosomes (Barral et al., 2022; Bright et al., 2016). To note, we were unable to define ‘A’ and ‘B’ type lysosomes on the basis of functional properties as described above (henceforth: ‘lysosomes of differentiated keratinocytes’). Dextran-fluorescein (70 KDa) is another soluble cargo that accumulates in the terminal endocytic compartments or lysosomes. Uptake of dextran followed by LAMP1 co-staining revealed significant accumulation of dextran in control keratinocytes. However, the accumulation of dextran- in differentiated keratinocytes was not regular (Fig. 1G). This might be due to the less uptake/internalization of dextran beads in differentiated cells. Taken together, the lysosome population of control and differentiated keratinocytes possess molecular properties of conventional lysosomes.

Dispersed Golgi stacks remain closely apposed with the lysosomes in differentiated keratinocytes

Golgi disperses during *in vitro* differentiation of primary keratinocytes (Mahanty et al., 2019) and, in the differentiated layers of the epidermis *in vivo* (Yamanishi et al., 2019). We observed highly dispersed Golgi stacks in differentiated compared to the perinuclearly arranged Golgi stacks in control keratinocytes (Fig. S2A). Accordingly, conventional EM (not shown) and, EM analysis of ultrathin cryosections revealed more compact Golgi structure with a few characteristic buds/vesicles in control keratinocytes. On the other hand, the Golgi in differentiated keratinocytes was highly dispersed with an enormous number of vesicles (Fig. S2B). In spite of Golgi dispersion, the association between *cis*-Golgi marker

GM130 and *trans*-Golgi marker p230 (Figs. 2A and S2A; first panels) was unaltered which suggests functional dispersion of Golgi during keratinocyte differentiation (Rambourg et al., 1993; Thayer et al., 2013). To test our hypothesis, control and differentiated keratinocytes were stained with wheat germ agglutinin-A594 (hereafter WGA) which binds to the plasma membrane (PM) bound sialic acid (SA) and N-acetylglucosamine (GlcNAc) , secreted from the Golgi. Hence, the PM binding of WGA is an indirect measure of Golgi function (Xiang et al., 2013). WGA binding to the PM was prominent or even more in differentiated compared to the control keratinocytes (Fig. S2D), suggesting dispersed Golgi stacks are functional in differentiated keratinocytes.

On the basis of comparable intracellular distribution of lysosomes and Golgi, we hypothesized an interconnection between these organelles. Accordingly, IFM analysis between the lysosome marker LAMP1 with the Golgi markers (representing separate Golgi regions) was performed. As shown, all the Golgi markers showed close apposition with LAMP1, irrespective of their spatial localization in the Golgi (Fig. 2A, white arrowheads). Localization between *cis* -Golgi protein GM130 and *trans*-Golgi protein p230 was taken as a positive control in this analysis (Fig. 2A, first panel). The association between Golgi and lysosome was respectively quantified by measuring Pearson's correlation coefficient (r) and Mander's overlap coefficients (M1: lysosome overlap with Golgi, and M2: Golgi overlap with lysosome). As shown in Fig. 2A, GM130 labeled Golgi stacks were in close contact with the lysosomes (represented by white arrows) (r=0.25±0.01, M1=0.16±0.01 and M2=0.49±0.02), which was comparable to GM130 association with p230 (taken as positive control; r=0.32±0.01, M1=0.24±0.01 and M2=0.36±0.01). Similar to GM130, the frequent association of p230 with LAMP1 was also observed (Fig. 2A; r=0.29±0.01, M1=0.24±0.02, and M2=0.45±0.02). Although the correlation between TGN46 and LAMP1 was lower among the Golgi markers, the overlap of TGN46 (M2) was comparable to other Golgi markers (Fig. 2A; r=0.20±0.01, M1=0.19±0.01, and M2=0.34±0.01). Expressed Arf1-GFP positive Golgi stacks have also shown a comparable association with LAMP1 (Fig. 2A; r=0.23±0.02, M1=0.17±0.01, and M2=0.38±0.02). In conclusion, Golgi proteins showed a higher overlap tendency with the lysosomes (but not in vice versa) in differentiated keratinocytes (refer to M1 and M2 values in respective graphs,Fig. 2A). A similar tendency was also observed in control keratinocytes, however, it may be due to the random overlap of Golgi with the lysosomes in the perinuclear area (Fig. S2A, control panels).

The differential overlap of *trans*-Golgi marker p230 (marked in green) with the *cis*-Golgi marker GM130 (marked in red) was unexpected as both these proteins localize to the Golgi complex (Fig. 2A, first panel M2value). To rule out the possibility of technical bias in the quantification method, the overlap between LAMP1 and LAMP2 (lysosome localized proteins) in control (bar graph in red, perinuclear organelles) and differentiated condition (bar graph in blue, dispersed organelles) was measured. As expected, no significant difference between M1 and M2 values was observed between the lysosomal markers LAMP1 and LAMP2 (Fig. S2E). Therefore, the spatial localizations of GM130 and p230 respectively to the *cis* and *trans* Golgi possibly contributed to the differential M2 values. Note that the association between LAMP1 and LAMP2 (as positive control; Fig. S2E; r=0.86±0.01, M1=0.82±0.02 and M2=0.85±0.02) and LAMP1-DAPI (as negative control; Fig. S2E, r=0.04±0.01, M1=0.01±0.00, and M2=0.02±0.01) were taken as controls for the overlap experiments. Altogether these data suggest that dispersed Golgi and lysosomes are in close apposition in differentiated keratinocytes.

Next, towards a better understanding of the association between Golgi and lysosome, electron microscopy experiment was performed. As shown, keratinocyte lysosomes appear in different morphologies, therefore we first defined the lysosomes by LAMP1 immunogold labeling of ultrathin cryo-sections (Fig. S2C). We considered a bilayered organelle as lysosome by the presence of atleast two LAMP-1immunogold (Fig. S2C). TEM analysis of the ultrathin cryo-sections has further revealed a significant overlap of vesiculated Golgi with the lysosomes in differentiated keratinocytes (Fig. 2B, right panel, black arrowheads). Approximately 70% of the lysosomes in differentiated keratinocytes were in close apposition (within 100 nm) to the Golgi compared to only 18% in control keratinocytes (Fig. 2C). Further, quantification of the distance (nm) between the lysosome membrane and nearest Golgi membranes (vesicles/stacks) revealed a regular distribution between these organelles (within≤50 nm) in differentiated keratinocytes, compared to a random and wide distribution in control keratinocytes. Collectively, these results confirm a close physical proximity or overlap between Golgi and lysosomes in differentiated keratinocytes.

Functional Golgi is essential for the generation of keratinocyte lysosomes

Small GTPase Arf1 regulates the generation of COPI vesicles which mediate intra-Golgi transport and Golgi – ER retrograde transport (Spang, 2002; Yang et al., 2011). To follow the Golgi dynamics and its role in the generation of lysosomes, GFP -tagged Arf1 was co-expressed with LAMP1-RFP. Arf1-GFP was localized to the dispersed Golgi stacks and to unique small tubulo-vesicular structures in differentiated keratinocytes (Fig. 3A). Arf1-positive tubulo-vesicular structures were highly dynamic and frequently seen contacting/fusing with the lysosomes (Fig. 3A, arrowheads and Video S2) both in time series and steady state (Fig. 3B) experiments. Accordingly, Arf1 association to the lysosomes was also not significantly altered between live and steady state (Fig. 3C in live r=0.25±0.03; Fig. 2A last panel in steady state r=0.23±0.02) in differentiated keratinocytes. Although, very less in number, small tubulo-vesicular structures were also observed in control keratinocytes (arrowheads Figs. S3A, Video S3 and, S3B r=0.27±0.03). Interestingly, the small Arf1-positive LAMP1-structures were specific to keratinocytes and not observed in other cell types for example HeLa (data not shown). Additionally, the expression of GFP alone or any other Golgi associated proteins did not generate similar structures, which confirms the specificity of Arf1 in the generation of tubulo-vesicular compartments. To validate the role of Arf1 in the production or maintenance of keratinocyte lysosomes, GFP-tagged dominant negative mutant of Arf1 (Arf1^{T31N}-GFP) was co-expressed with LAMP1-RFP. As expected, Arf1^{T31N}-GFP localized to the cytosol with a complete abolition of its localizations to the Golgi stacks and to tubulo-vesicular structures. Interestingly, expression of Arf1^{T31N}-GFP led to a complete loss of the lysosomes and, as shown LAMP1-positive tiny punctate structures accumulated in the perinuclear area (Fig. 3D, arrows, and arrowheads). In line, the Golgi was also appeared punctated in the differentiated keratinocytes expressing Arf1^{T31N}-GFP mutant (Fig. S3C). However, perinuclear localized lysosomes of control keratinocytes were not significantly affected by the expression of Arf1^{T31N}-GFP (Fig. S3D).

The effect of Arf1 inhibition was further verified by using pharmacological inhibitors. Brefeldin A (BFA) inhibits Golgi function by inhibiting the Arf1 mediated assembly of COPI vesicles (Kawamoto et al., 2002; Presley et al., 1998). The ubiquitous function of Arf1 is mediated by its activation through specific GEFs (Guanine exchange factors). For instance, GBF1 (Golgi-specific brefeldin A-resistance guanine nucleotide exchange factor 1) localizes to the *cis*-medial Golgi and regulates COPI vesicle assembly through Arf1 (Garcia-Mata et al., 2003; Kawamoto et al., 2002; Manolea et al., 2008); BIG1 and BIG2 (Brefeldin A -inhibited guanine nucleotide exchange proteins) localize to the late

Golgi and regulate the membrane traffic between TGN and endosomes (Ishizaki et al., 2008; Manolea et al., 2008; Walton et al., 2020). Hence, Arf1 function can be selectively inhibited by specific inhibition of Arf1-GEFs (Fig. 3E). Treatment of primary keratinocytes with BFA (0.4 μg/ml for 6 - 24 h) or golgicide A (GCA, GBF1 inhibitor, 50 μM for 6 - 24 h) led to the dissociation of Golgi membrane as expected (Fig. 3F). Surprisingly, both BFA and GCA treatments also led to complete dissociation of the lysosomes in differentiated cells (Fig. 3F). In contrast, EXO-II treatment in differentiated keratinocytes (BIG1/2 inhibitor, 20 μM for 6 - 24 h) led to the dissociation of Golgi but not the lysosomes (Fig. 3F). These results suggest a specific role of COPI in the generation of keratinocyte lysosomes. The dispersion of LAMP1-positive lysosomes upon brefeldin A or GCA treatment was also observed in control keratinocytes (Fig. S3E), but not in other cell types like HeLa or primary fibroblasts (not shown). Further, the cell surface binding of WGA (an indicator of Golgi function) was completely blocked in brefeldinA treated differentiated and control keratinocytes (Fig. S3F). In addition, WGA positive granules (representing the *trans*-Golgi carriers) were also dissociated as similar to lysosomes in differentiated keratinocytes (Fig. S3F). Taken together, these data support the role of functional Golgi or Arf1/COPI mediated Golgi function in the generation of keratinocyte lysosomes.

Peripheral Golgi protein GRASP65 surrounds the lysosomes in differentiated keratinocytes

GRASPs (GRASP65 and GRASP55) are the peripheral Golgi proteins localize respectively to *cis* and medial-*trans* Golgi, and regulate Golgi ribbon morphology through oligomerization (Satoh et al., 2015; Xiang and Wang, 2010). A role of GRASPs in the dispersion of Golgi in differentiated keratinocytes was suspected. However, no significant change was observed in the mRNA or protein levels of GRASP55 and GRASP65 in differentiated compared to the control keratinocyte (data not shown). Neither individual nor co-expression of GRASP65/55 could reverse the Golgi morphology in differentiated keratinocytes (Fig. S4A). Co-expressed GRASP55 and GRASP65 localized to the dispersed Golgi stacks (Fig. S4A) and the pattern of Golgi dispersion was similar to the endogenous pattern of Golgi in differentiated keratinocytes (Fig. S4G). Altogether, these results do not suggest the direct involvement of GRASPs in regulating the Golgi morphology in differentiated keratinocytes. Interestingly, overexpressed GRASP65 appeared in unique ring-like structures in addition to its localization to dispersed Golgi stacks and a cohort to the cytosol (Fig. 4A, arrows, and arrowheads). To note, the GRASP65 ring-like structures were not positive for GRASP55 (Fig. S4A) or for other Golgi proteins such as Arf1 (data not shown). Further, the ring-like structures were present in approximately 95% of the differentiated keratinocyte expressing GRASP65-GFP as compared to approximately 9% in control keratinocytes (Figs. 4B and S4C). To mention, GRASP65-GFP ring-like structures were best visible in live cell experiments (~94% of the cells), were less intact in the steady state (~60% of the cells), and were not visible (~0.1% in IFM) by endogenous staining of GRASP65 (Figs. 4B and S4G). We hypothesize these GRASP65 ring-like structures are possibly the fixative sensitive structures, as described for GFP-GM130-positive intermediate compartments (Marra et al., 2001).

Interestingly, the GRASP65 ring like structures surrounded the lysosomes of differentiated keratinocytes when co-expressed with the lysosome marker LAMP1-RFP (Fig. 4A, arrowheads; Video S4). Accordingly, the perimeter of the GRASP65-GFP rings (denoted as G; 37.9±1.3 pixels) was significantly higher than the LAMP1-RFP rings (denoted as L; 25.3±1.1 pixels) (Fig. 4C). The Pearson's correlation coefficient between GRASP65 and LAMP1 was higher in live (r=0.54±0.03) than that of steady state (r=0.39±0.02) in differentiated keratinocytes, which further confirmed the fixative sensitivity of GRASP65

structures (Figs. 4E and 4D). The overlap coefficient of GRASP65 to the lysosomes (M2 values, and not vice versa) was also significantly higher (both in live and steady), supporting the higher overlap tendency of Golgi proteins to the lysosomes (as described in Fig. 2) (Figs. 4D and 4E). In contrast, GRASP65 rings were extremely rare in control keratinocytes (~ 9% of cells having one or two rings/cell) (Figs. S4B and S4C; Video S5). Accordingly, due to the extremely rare appearance of GRASP65 rings, Pearson's correlation remained unaltered between live and steady states (r=0.44±0.02 in live and 0.47±0.03 in steady; Figs. S4E and S4D) in control keratinocytes. In addition to maintaining the Golgi ribbons, GRASP proteins especially GRASP55 mediates unconventional secretion from autophagosomes (reviewed in (Giuliani et al., 2011; Zhang and Wang, 2020). GRASP55 was also shown to interact with LAMP2 and LC3II to facilitate lysosome-autophagosome fusion during glucose deprivation (Zhang and Wang, 2018). We have tested the possibility of these LAMP1-positive structures as autophagosomes by co-immunostaining of LAMP1 with LC3-II. But, no significant association of LC3-II to the LAMP1-positive structures was observed in control and differentiated keratinocytes (Fig. S4F, arrowheads), indicating that these LAMP1-positive structures are not autophagosomes. Overall, these studies revealed that Golgi peripheral protein GRASP65 surrounds the lysosomes of differentiated keratinocytes.

Next, we analyzed the GRASP65 ring like structures and their association with the lysosomes by structured illumination microscopy (SIM) in differentiated keratinocytes co-expressing GRASP65-GFP and LAMP1-RFP. Unlike complete ring like structures of GRASP65 in Airyscan super resolution microscopy (Fig. 4A), GRASP65-GFP in SIM imaging appeared as distinct patches arranged on the periphery of the lysosomes and revealed discontinuous when images were evaluated after the 3D rendering of the lysosomal structures (Figs. 4F and 4G). The average number of GRASP65 per lysosome ranged between 1 to 3. Further, the length and breadth values of GRASP65-positive Golgi structures and LAMP1-positive lysosome structures showed independent distribution (Figs. 4H and 4I), which confirms the specificity of GRASP65 association with the lysosomes (Fig. 4F). Together, the peripheral Golgi protein GRASP65 localized as distinct patches to the lysosome membrane in differentiated keratinocytes.

Furthermore, the immunogold labeling of ultrathin cryosections of differentiated keratinocytes also revealed the presence of GRASP65 on the lysosomes (Fig.4J). As expected, the majority of the GRASP65 immunogold was present to the Golgi and Golgi vesicles (GVs) (65±8%) (Figs 4J and 4K). In addition, a small fraction was also present on the lysosomes (27±7%) (Figs 4J and 4K), and negligible numbers in the nucleus and mitochondria (not shown). To note, approximately 46% of the lysosomes were positive for GRASP65 with an average frequency of one GRASP65 immunogold per lysosome (Fig. 4J). Altogether, these results confirm the presence of GRASP65 on the periphery of lysosomes in differentiated keratinocytes.

GRASP65 mediates Golgi-lysosome contact in differentiated keratinocytes

Golgi tethering protein GRASP65 remains attached to the *cis*-Golgi membrane by myristoylation at its N-terminus and through interaction with golgin GM130 on another side (reviewed in (Zhang and Wang, 2015). We assessed the possible functional significance of GRASP65 association with keratinocyte lysosomes by siRNA mediated inhibition approach. To examine if GRASP65 association with the lysosome membrane was also dependent on GM130, specific siRNA mediated inhibition of GM130 was performed. siRNA specific to GRASP55 was taken as a control of GRASP65 siRNA inhibition. We observed more than 70% inhibition of GRASP65 and GRASP55 with respective siRNAs in primary keratinocytes (Fig. S5D). The knockdown of GM130, GRASP55 and GRASP65 was also confirmed by

IFM using specific antibodies (Figs. S5A, S5B and S5C) and by immunoblot of GRASP65 (Fig. S5E). Inhibition of any of these proteins in differentiated keratinocytes did not enhance the Golgi dispersion compared to control siRNA (Fig. 5A, data not shown). Further, visual analysis of Golgi stack morphology in the individual knockdowns of GRASP65, GRASP55 and GM130 compared to the control siRNA was inconclusive (except comparatively bigger stack size of Golgi in siGRASP65 cells in Fig. 5A) (data not shown). This may be due to the variation in the differentiation state and efficiency of knockdown in the respective cells. Interestingly, the inhibition of GRASP65 but not GRASP55 resulted in the prominent loss of Golgi-lysosome contacts (Fig. 5B, arrows). In line, the distance between Golgi stacks and lysosomes became more random and significantly higher in siGRASP65 cells compared to the siControl or siGRASP55 cells (Fig. 5C).

Next, analysis of lysosome morphology revealed the presence of prominent giant sized and tubular LAMP1-positive structures in GRASP65 knockdown cells compared to the control siRNA treated cells (Fig. 5A, arrow and arrowheads). Interestingly, we did not observe any significant visual change in the lysosome morphology in siGRASP55 or in siGM130 (Fig. S5A and S5C) compared to control siRNA treated cells(Figs. 5A and S5B). To understand the characteristic giant-sized perinuclear LAMP1-positive membranous structures in siGRASP65 cells, we tested for the presence of LR, dextran-fluorescein and Arl8B. Interestingly, these structures were positive for LR and dextran-fluorescein but not for Arl8B (Figs. 5D and S5F). This result in particular suggests that the characteristic giant structures are acidic compartments, but not mature lysosomes. In accordance, the accumulation of the substrate of lysosomal hydrolase beta-glucocerebrosidase was observed (Fig. 5D 3rd panel arrows and, S5F, 3rd panel). Additionally, CD63 which decorates the membrane of keratinocyte lysosomes (Fig. 1A), was found interior to these compartments. Although future investigation is required, together, these results suggest a block in the maturation of lysosomes which in turn resulted in the accumulation of giant acidic membranous compartments. Accordingly, the volume distribution analysis of organelles in siGRASP65 keratinocytes revealed a significantly higher volume of LAMP1-positive compartments compared to the siControl cells (Fig. 5E). To note, the inhibition of GRASP65 in control keratinocytes did not have a significant effect on the lysosomes (not shown). Altogether, these data suggest a functional role for GRASP65 in mediating the close apposition between Golgi and lysosome, required for the maturation of lysosomes in differentiated keratinocytes.

Keratinocyte lysosomes originate from the *trans*-Golgi

To understand the functional significance of Golgi to lysosome cross talk as discussed above, we examined the localization of Golgi resident cargo enzymes and, intracellular trafficking of secretory Golgi cargo neuropeptide Y (NPY) and VSVG (vesicular stomatitis virus G glycoprotein). β-1,4 galactosyltransferase1 (galT) is a *trans*-Golgi resident enzyme which is shown to be often localized in *trans*-Golgi derived vesicles and traffic to other endocytic compartments and to plasma membrane (Schaub et al., 2006). In lieu of this, the dynamic localization of galT and the medial Golgi enzyme ManII was examined with respect to the LAMP1 positive lysosomes of differentiated keratinocytes. Co-expression of ManII-GFP along with LAMP1-RFP revealed the presence of ManII GFP exclusively to the dispersed Golgi stacks in close apposition to the lysosomes (Fig. S6A). In contrast, besides localization to the dispersed Golgi stacksa major fraction of galT-RFP was also localized to the lumen of lysosomes and appeared as bright round structures in differentiated keratinocytes (Fig. 6A, white arrows and arrowheads) surrounded by LAMP1-GFP. Accordingly, galT immunogold labelling of ultrathin cryosections revealed the presence of galT to the interior of

approximately 47% of the lysosomes in differentiated keratinocytes, with a frequency of 1 to 3 beads per lysosome (Fig. 6B). Unlike GRASP65 distribution, the distribution of galT immunogold to the lysosomes was equal to that of the Golgi and Golgi vesicles, indicating a shift in galT localization when compared to GRASP65 localization (Fig. 6C and Fig. 4K). The presence of galT immunogold to other organelles such as in nucleus and mitochondria was negligible (data not shown). Taken together, these results confirmed the presence of *trans*-Golgi enzyme galT to the lumen of the lysosomes of differentiated keratinocytes. Next, we analyzed the trafficking of ectopically expressed secretory cargoes NPY and VSVG. Previously it was shown that Golgi to PM transport of NPY is mediated by the *trans* Golgi derived secretory vesicles (Grigoriev et al., 2007; Patwardhan et al., 2017).These *trans*-Golgi derived vesicles are also positive for secretory cargo VSVG and small GTPase Rab6 (Grigoriev et al., 2007; Patwardhan et al., 2017).

Strikingly, we observed NPY positive vesicles correspond to the lysosomes in differentiated keratinocytes which were also positive for VSVG (Fig. 6E, panel1, panel 2). The extent of localization of NPY or VSVG to the lysosomes was comparable to that of secretory/exocytic vesicles as described in other cell types (Grigoriev et al., 2007). To note, at times a small fraction of lysosomes in control keratinocytes also appeared positive for NPY and galT (~ 14% of cells), however in the majority of the control cell population lysosomes were not positive for NPY, VSVG or galT (Fig. 6E). Taken together, these results suggest that lysosomes in differentiated keratinocytes are modified from the *trans*-Golgi carriers.

Discussion:

Keratinocytes differentiate in response to increasing calcium gradient in the upper skin layers (Bikle et al., 2012; Hennings et al., 1989). During late stages of differentiation, keratinocytes lose conventional intracellular organelles including their nuclei, while generating specialized organelles respectively required for cornification and skin barrier homeostasis (Akinduro et al., 2016); reviewed in (Mahanty and Setty, 2021). Increased autophagy in the upper skin layers contributes to organelle removal which may also sustain the nutrient deficient environment (Akinduro et al., 2016; Yoshihara et al., 2015). However, the functional status of lysosomes in the epidermal sublayers remains unknown. Lysosomes are dynamic organelles that change molecular and functional properties to adapt to cellular demand besides their conventional role in degradation (Ballabio and Bonifacino, 2020). Recent reports highlight the critical role of lysosomes in skin epidermis homeostasis (Bochenska et al., 2019; Monteleon et al., 2018). We have previously reported increased biogenesis and peripheral distribution of lysosomes during *in vitro* differentiation of human primary keratinocytes. The biogenesis of keratinocyte lysosomes does not follow a conventional mTOR-regulated TFEB/TFE3 pathway, instead it relies on an ER stress regulated UPR pathway (Mahanty et al., 2019). Of note, the increased lysosome biogenesis during differentiation accompanies the dispersal of the Golgi apparatus (Mahanty et al., 2019). However, the molecular properties of keratinocyte lysosomes and the possible correlation between lysosome biogenesis and Golgi dispersion remained unexplored. In this study, we provide evidence of the involvement of Golgi to the generation of keratinocyte lysosomes and acquisition of their unconventional properties. These unique properties of keratinocyte lysosomes are denoted by the presence of *trans*-Golgi enzyme galT in the lumen, selective accumulation of secretory cargoes upon expression, reversible dissociation of the lysosomes in presence of brefeldin-A and, finally a critical loss of the lysosomes upon Golgi inhibition. Unlike conventional lysosomes in HeLa or in primary fibroblasts we show that the lysosomes of differentiated keratinocytes remain closely apposed with the dispersed Golgi stacks which is critical for their maturation. We hypothesize that the unconventional properties of

keratinocyte lysosomes are likely to contribute to the higher secretory demand of differentiating keratinocytes in the epidermal sublayers (Boyce, 1994; Katz and Taichman, 1994).

The fundamental trafficking mechanisms involved in intracellular organelle biogenesis and homeostasis remain exceptionally unknown in epidermal keratinocytes. For instance, in *in vivo* differentiating epidermal sublayers and, *in vitro* differentiating keratinocytes, the Golgi apparatus is redistributed throughout the cytosol (Mahanty et al., 2019; Yamanishi et al., 2019). But the mechanisms underlying such alteration in Golgi morphology in keratinocytes and, its functional significance remains unclear. Previous studies in other cellular systems show Golgi dispersion in presence of high calcium (Ireland et al., 2020), during mitosis (Colanzi and Corda, 2007), in loss of adhesion (Singh et al., 2018), and also during differentiation (Kreft et al., 2022; Wei and Seemann, 2017) involving different molecular pathways/mechanisms. As keratinocyte differentiation is achieved in presence of high calcium, we hypothesized a possible role of high calcium induced Golgi dispersion through PKC alpha mediated phosphorylation of GRASP55 (Ireland et al., 2020). The essential roles of GRASP55 and GRASP65 in regulating Golgi ribbon morphology are well established (Colanzi and Corda, 2007; Xiang and Wang, 2010). However, in this study, we did not observe a significant change in the expression of these molecules during differentiation (unpublished data), nor the individual or co-expression of these molecules could rescue the Golgi dispersal phenotype, suggesting that Golgi dispersion in differentiating keratinocytes involves a separate mechanism.

As stated above, the function of GRASPs especially GRASP65 is likely to be remodeled to support the lysosome biogenesis through its tethering role in differentiating keratinocytes. Since Golgi dispersal favors the close apposition with the lysosomes, the conventional role of GRASP65 to maintain Golgi ribbon is disadvantageous in keratinocytes. Here we show that GRASP65 mediates the Golgi-lysosome apposition and thereby supports lysosome maturation. In line, GRASP65 inhibition results in the loss of Golgi-lysosome apposition and accumulation of LAMP1-positive giant membranous acidic compartments. These compartments accumulate lysosome substrate glucosylceramide and are negative for Arl8B, indicating a defect in lysosome maturation (Khatter et al., 2015). On the basis of these results, we hypothesize multiple tethering roles of GRASP65 in receiving cargo containing vesicles from the Golgi by maintaining Golgi-lysosome close apposition, which in turn, is necessary for the maturation of the lysosomes. On the other hand, the increased size of the LAMP1 positive compartments may either be due to the affected fission of the lysosomes or the accumulation of cargo due to a block in secretion. GRASP proteins especially GRASP55 is shown to be involved in unconventional secretion from the autophagosomes (Giuliani et al., 2011; Nickel, 2010), which is not likely in the current context as keratinocyte lysosomes do not show significant association with either GRASP55 or LC3-II. Although we did not examine the direct role of GRASP65 influence in the secretory capacity of lysosomes in differentiated keratinocytes, we did observe an enhanced expression of LAMP1 at the cell surface in a significant population (36%) of GRASP65 overexpressing cells (not shown). On the basis of these results, we speculate an involvement of GRASP65 in the secretory properties of keratinocyte lysosomes or in the tethering of these specialized lysosomes with the plasma membrane for regulated exocytosis (Rabouille and Linstedt, 2016).

Accordingly, selective and extensive accumulation of the secretory cargoes NPY and VSVG to the LAMP1 positive lysosomes, suggest these lysosomes as the modified *trans*-Golgi derived exocytic carriers (as described in (Grigoriev et al., 2007). The presence of *trans* -

Golgi enzyme galT in the lumen of these lysosomes further supports our conclusion. Moreover, keratinocyte lysosomes show a reversible dissociation in presence of Golgi functional inhibitor brefeldin A. In line, the generation of these lysosomes in differentiated keratinocytes is critically dependent on the Golgi function, which is unique in these cells. In order to alter Golgi function, we modulated Arf1 expression as Arf1 is a critical regulator of Golgi that functions by regulating intra-Golgi transport through the generation of COPI coated vesicles (Donaldson et al., 2005; Spang, 2002). Besides this regulation, Arf1 is also a structural component of COPI coated vesicles (Spang, 2002; Yang et al., 2011). Expression of Arf1 -GFP generates small dynamic vesicular structures (possibly COPI vesicles) which fuse with the lysosomes (Fig. 3A). Interestingly, the expression of a dominant negative mutant of Arf1 ($Arf1^{T31N}$-GFP) results in the critical loss of lysosomes with the loss of Arf1 positive dynamic vesicular structures. However, the expression of Arf1 in other cell types like HeLa that harbor conventional lysosomes do not display dynamic vesicular structures and, the expression of $Arf1^{T31N}$-GFP had no effect on the lysosomes (unpublished data), reinforcing the unique characteristics of keratinocyte lysosomes. Previous studies show that Golgi dispersion multiplies functional units through localized synthesis and transport of proteins, which support higher secretion by generating higher COPI vesicles (Hanus and Ehlers, 2008; Wang et al., 2008). As GBF1/Arf1 axis generates COPI coated vesicles and the latter is sensitive to brefeldin A (Kawamoto et al., 2002; Nebenfuhr et al., 2002), we hypothesize an involvement of COPI in the generation/maintenance of keratinocyte lysosomes. However, whether functional coordination exists between Arf1 and GRASP65 is yet to be investigated.

Taken together, based on these results, we propose that during keratinocyte differentiation specialized lysosomes generate from the Golgi followed by their maturation through constant Golgi input likely to be mediated by COPI coated vesicles (Fig. 6F). Golgi dispersion promotes the generation of COPI vesicles by GBF1-mediated Arf1 activation. Close Golgi-lysosome apposition mediated by the Golgi tether GRASP65 facilitates receiving of COPI vesicles (Fig. 6F). We believe that the generation of specialized lysosomes is an adaptation to the nutrient deficient environment in the upper skin layers, that is likely to serve the dual purpose of degradation and secretion required to maintain epidermis homeostasis.

Material and methods

Chemicals and fluorescence substrates: All the chemicals and reagents used in this study were purchased from Sigma-Aldrich (Merck) or ThermoFisher Scientific (Invitrogen) unless mentioned. LysoTracker Red DND-99 (L7528) and Wheat Germ Agglutinin (WGA)-Alexa Fluor 594 (W11262) were obtained from ThermoFisher Scientific (Invitrogen). Dextran-Fluorescein (70K MW, D1822), brefeldin A (B7651), Golgicide A (G0923) and EXOII (E7159) were procured from Sigma-Aldrich. Trypsin and trypsin neutralizer solution were obtained from ThermoFisher Scientific (Invitrogen). Collagen-I was obtained from BD-Biosciences. N-C6:0-NBD-glucosylceramide was from Matreya LLC, USA. Lipofectamine 3000 and oligofectamine were obtained from ThermoFisher Scientific (Invitrogen).

Antibodies: Following polyclonal and monoclonal primary antibodies were used (abbreviations, m=mouse; h=human and r=rat proteins). Abnova: anti-GALT (PAB31346). BD Biosciences: anti-rGM130 (610822) and anti-hp230/golgin-245 (611281). BioRad: anti-hTGN46 (AHP500G). Cell Signaling Technology: anti-LC3A/B (4108). Developmental Studies Hybridoma Bank: anti-hCD63 (H5C6), anti-hLAMP-1 (H4A3) and anti-hLAMP-2 (H4B4). Invitrogen: anti-LAMP1 (14-1079-80). Merck: anti-hCathepsin D (IM16).

Proteintech: Arl8b (13049-1). Santa Cruz biotechnology: anti-GAPDH (sc-25778), anti-hGRASP55 (sc-365602) and anti-hGRASP65(sc-365434). All secondary antibodies were either from Invitrogen or Jackson Immunoresearch.

Primers, siRNAs and plasmids:

Primers used for qRT-PCR analysis		
Gene name	Forward (5'-3')	Reverse (5'-3')
h*GRASP65*	GGGCCAGAGGACATCTGCTC	TGTGGTAGAGATCTGGGCCTG
h*GRASP55*	GTTGGCTTACCAGAACTTGT	AGGTGACTCAGAAGCATTGG
h*18S rRNA*	TTTCGGAACTGAGGCCATGA	GAACCTCCGACTTTCGTTCTTGA

The following target siRNA sequences were synthesized from Eurogentec, Belgium. hGRASP65 (5'-GAUCUCUACCACAGAAUAA-3'), hGRASP55 (5'-GAGUCUGACUGGACUUUCU-3') and hGM130 (5'-GAAUCAUGAUGCUGACAAU-3'). Control siRNA was also procured from Eurogentec. Following plasmids used in this study were described previously: $Arf1^{WT}$-GFP, $Arf1^{T31N}$-GFP (Kumari and Mayor, 2008); GRASP55-GFP, GRASP55-mCherry and GRASP65-GFP (Zhang et al., 2018); LAMP1-GFP (Marwaha et al., 2017); galT-RFP and ManII-GFP (Singh et al., 2018); NPY-Venus (Patwardhan et al., 2017). LAMP1-RFP was obtained from Addgene. VSVG-GFP was a kind gift from Dr. Bruno Goud Institute Curie.

Primary keratinocyte culture and differentiation: Human neonatal primary keratinocytes were purchased from Lonza, Invitrogen or Life line Cell Technology and grown according to manufacturer's instructions. Cells were maintained and passaged in the respective medium and used until passage four (P4). For differentiation, cells were grown to 50 - 60% confluence and $CaCl_2$ was added to the culture medium to a final concentration of 2 mM. Cells were incubated for 48-60 hours with changing of medium in every 24 h. We have used bigger cell size and dispersal of lysosomes as differentiation characteristics as described previously (Mahanty et al., 2019).

Dextran-Fluorescein, LysoTracker Red DND-99 and NBD-Glucosylceramide uptake: Glass coverslips containing control and differentiated keratinocytes were incubated in fresh culture medium with 0.5 mg/ml of dextran-fluorescein for 6 h (included in the total differentiation time) or 50 –75 nM of LysoTracker Red for 10 min in a 37°C incubator with 10% CO_2. After incubation, the coverslips were washed twice with 1X PBS, fixed with 4% PFA and stained for LAMP1. For NBD-Glucosylceramide (NBD-GCS) uptake, the cells on glass coverslips were first washed with 1XHBSS/HEPES buffer and incubated with a final concentration of 2 μM NBD-GCS in 1XHBSS/HEPES at 4°C for 30 min to promote its binding. After 30 min, the dye was removed, washed twice with HBSS/HEPES buffer and incubated in fresh growth medium for at least 30 min at 37°C in an incubator maintained with 10% CO_2. Cells were then washed in fresh medium and either imaged in live or, fixed with 4% PFA and imaged.

Gene expression and siRNA mediated inhibition in primary keratinocytes: For the expression of fluorescent protein tagged constructs, Lipofectamine 3000 was used as per the manufacturer's instruction. The cells were imaged in between 36 – 48 hours of transfection. Transfection of specific siRNA was performed by using oligofectamine as per the manufacturer's protocol. Briefly, primary keratinocytes at ~ 60% confluence were transfected in serum free medium. A final concentration of 20 nM of siRNA was added to the cells and

incubated till 72 h. To achieve the differentiation, cells were added with calcium post 24 h of siRNA transfection and then incubated for another 48 h.

Small molecule treatment and differentiation: Primary keratinocytes were grown on glass coverslips to 50 – 60% confluence. The compounds/drugs or respective solvent (as a control) was added to the medium in duplicates. After 3 hours of treatment, the coverslips were segregated into two sets for control and differentiated conditions. The later set of coverslips was added with $CaCl_2$ to a final concentration of 2 mM. All coverslips were incubated for 24h along with the indicated concentrations of compound/solvent to avoid reversal of the phenotype. Cells were then fixed with 4% PFA and continued for immunostaining.

Gene expression by qRT-PCR analysis: For these experiments, siRNA-mediated gene knockdown was performed in 35 mm dishes. RNA was isolated using GeneJET RNA purification kit (ThermoFisher Scientific) followed by cDNA preparation using cDNA synthesis kit (Fermantas). Same cDNA was used to amplify both the gene of interest and *18S rRNA* in Quant-Studio 6 Flex real-time PCR system (Applied Biosystems). The PCR conditions consisted of AmpliTaq Gold activation at 95°C for 10 min, followed by 40 cycles of denaturation at 95°C for 20s, annealing at 58°C for 25s and extension at 72°C for 30s. A dissociation curve was generated at the end of each cycle to validate the single transcript amplification. The change in SYBR green fluorescence intensity was monitored and then calculated the threshold cycle (C_t) number. The C_t value of the gene was subtracted from respective control to obtain the ΔC_t value. The ΔC_t value of treated sample was subtracted with the ΔC_t value of control to obtain the $\Delta\Delta C_t$ value. The gene expression level in the knockdown conditions in compared to the control was expressed as $2^{-\Delta\Delta Ct}$ values from three independent experiments, and plotted as mean±s.e.m. (considering control as 1.00).

Immunostaining and immunoblotting: Immunostaining of the cells was performed as described previously (Mahanty et al., 2019). Briefly, 4% PFA fixed cells were simultaneously permeabilized and immunostained by incubating in the primary antibody solution containing saponin. Cells were incubated with primary antibody at room temperature for approximately 1h followed by incubation with the respective Alexa fluor conjugated secondary antibody for 20-30 min. For WGA-AF594 staining, 4% PFA fixed cells were incubated with 100µM of WGA-AF594 in 1XPBS for 10 min at RT, followed by staining for LAMP1. For immunoblotting, cell lysate was prepared in SDS lysis buffer and then subjected to immunoblotting analysis as described previously (Mahanty et al., 2019).

Fluorescence microscopy: Most of the images including live cell experiments were performed under confocal laser scanning microscope with Airyscan super resolution module (ZEISS LSM 880 with Airyscan) at 63X magnification. Imaging was also done under spinning disk confocal microscope (Inverted Eclipse Ti-E (Nikon), Spinning disk CSU-X1 (Yokogawa)) and, Olympus IX81 motorized inverted fluorescence microscope equipped with a CoolSNAP HQ2 (Photometrics) CCD camera.

Data analyses in ImageJ/Fiji: Analysis of the cell area, size, numbers and, perimeter of the lysosomes (in μm^2) was performed by using the watershed function. Lysosome numbers/μm^2 area was calculated by dividing total number of lysosomes by area of the respective cell. Pearson's colocalization (*r*), and Mander's overlap coefficients (M1 and M2) was calculated using JaCoP plugin. Images were captured in Olympus IX81 motorized inverted fluorescence microscope to calculate localization coefficients. The nm distance between the Golgi

membrane to lysosome membrane and, Golgi stacks to lysosomes (Figs. 2D and 5C) were measured after respective scale calibration.

Structured Illumination Microscopy, 3D rendering and, analysis of length and breadth: Structured Illumination Microscopy was performed using ZEISS Elyra 7 with Lattice SIM microscope with a lateral (x-y) resolution of ~120 nm and an axial (z) resolution of ~300 nm. Samples were imaged as 3D stack with an axial interval of 200 nm between focal planes and, at 63X magnification. The images were reconstructed and rendered with the help of 4-D viewer in Metamorph 7.0 (Molecular Devices, USA) software.
For length and breadth analysis, Z-stack SIM micrographs of labelled lysosomes (LAMP1-RFP) and Golgi (GRASP65-GFP) were converted to maximum intensity projection. Using average + standard deviation values of fluorescence intensity of entire image, the signal was segmented to a binary image. The segmented image was used with integrated morphometric analysis tool to log length, breadth and area for the objects in Metamorph 7.0 (Molecular Devices, USA). Golgi and lysosomes of 3 differentiated keratinocytes from 3 different experiments were included. The number of organelles analyzed is mentioned on the respective graph. Independent values were plotted as a function of fractions and significance was analyzed by Mann-Whitney non-parametric analysis.

Volumetric analysis of lysosome and Golgi: Micrographs in Z-stack (imaged in Airyscan super resolution) of labelled lysosomes (LAMP1) and Golgi (GM130), were processed using 4D viewer module in Metamorph 7.0 (Molecular Devices, USA) (Previously reported in (Venkatachalapathy et al., 2019)). Micrographs were thresolded for intensity to segment the regions for the labelled lysosomes and Golgi for each focal image. With 4D viewer the structure was rendered and reconstructed to generate a 3D model of the Z-stack. Using filtering for size, appropriate lysosome and Golgi models were selected for volumetric analysis. Volume of individual objects detected was logged to CSV files and cumulative distribution was calculated using GraphPad Prism software (version 6.04). The value of significance was analyzed by Mann-Whitney non-parametric analysis between respective groups. Five cells of each category (control siRNA and GRASP65 siRNA treated cells) from 3 independent experiments were included in the analysis.

Cryo-sectioning, immunogold labelling and Transmission Electron Microscopy:
Ultrathin cryo sections were prepared and immunogold labelling was performed as described in (Hurbain et al., 2017). Briefly, the control and differentiated keratinocytes were fixed with 2% PFA and 0.25% Glutaraldehyde in 0.1 M phosphate buffer solution (pH 7.4) overnight at 4°C. Cells were embedded in 10% gelatin and cryoprotected by using 2.1M sucrose and stored in liquid nitrogen. Ultrathin cryosections (100nm) were prepared with an ultra-cryomicrotome UC7 FCS (Leica). Unlabelled cryosections were either processed for imaging after contrasting with uranyl acetate (as shown in Fig. 2B) or, processed for single/ double immunogold labeling with protein-A conjugated gold particles of 10 nm and 15nm diameter (Cell Microscopy Center, Department of Cell Biology, Utrecht University).Images were acquired with a Transmission Electron Microscope (Tecnai Spirit G2; ThermoFischer Scientific, Eindhoven, The Netherlands) equipped with a 4k CCD camera (Orius 1000, Gatan Inc., Pleasanton, CA). For all analyses ≥ 150 images from at least two different experiments were included.

Statistical analysis in graph pad prism (version 6.04): Cells from at least three independent experiments were included for statistical analysis (number of cells ‘n’ is

mentioned on the respective graph). Pearson's colocalization coefficient '*r*', and Mander's overlap coefficients M1 and M2 (mentioned together as 'localization coefficient') values were plotted as mean ± s.e.m. and the statistical significance was calculated by unpaired two tailed Student's *t*-test.

The non-normal distribution of Golgi to lysosome distances (Figs. 2D and 5Cwas analyzed by frequency distribution analysis. The value of significance was calculated either by Mann Whitney non-parametric test (between two samples) or by Kolmogorov-Smirnov non parametric test to analyze cumulative distributions specified in the respective sections. $*P \leq 0.05$, $**P \leq 0.01$, $***P \leq 0.001$, $****P \leq 0.0001$ and ns = non-significant. Graphs in 'red' color indicates control and 'blue' indicates differentiated conditions.

Figure legends

Figure 1. Comparative analyses of the lysosomes of control and differentiated keratinocytes. (**A**) IFM analysis of the lysosomes of LAMP1 stained control and differentiated keratinocytes. Two different morphologies of lysosomes 'A' and 'B' were observed in differentiated keratinocytes. Arrowheads point to the possible LAMP1 carriers. (**B**) significant increase in lysosome number/μm^2 in differentiated keratinocytes; n=number of cells. (**C**) average lysosome size (μm^2) is significantly increased in differentiated cells compared to control; n=number of lysosomes (**D**) the graph represents LAMP1 fluorescence intensity of A and B type lysosomes in differentiated keratinocytes; n=number of lysosomes (**E-G**) IFM analysis of control and differentiated keratinocytes that are co-immunostained for LAMP1 and CD63 (E), cathepsin D (F), or internalized dextran-fluorescein (G) and imaged under Airyscan super-resolution microscope. White arrows in the zoomed boxes point to the colocalization between the markers. White stars in panel F pointing cathepsin D negative LAMP1 compartments. In all images the insets represent 2.5 times magnified white boxed regions. Scale bar = 10 μm.

Figure 2. Golgi stacks and lysosomes are closely apposed in differentiated keratinocytes. **A**) IFM analysis of the differentiated keratinocytes co-stained either for the Golgi markers GM130 and p230 or, lysosome marker LAMP1 with the Golgi markers GM130 (representing *cis*/medial Golgi), p230, TGN46 or expressed Arf1-GFP. Cells were visualized under Airyscan super-resolution microscope. Represented insets are the 2.5 times magnified numbered (1-3) regions of the cells shown in Fig. S2A. Arrowheads represent the close apposition/contact between Golgi and lysosomes. Scale bar =2.5 μm. Pearson's correlation coefficient (*r*) and Mander's overlap coefficients (M1 and M2) were calculated in differentiated cells from at least 3 different experiments. n= number of cells. **** on the graphs indicates significant difference between M1 and M2 values. (**B**) Ultrathin cryosections of control and differentiated keratinocytes were analyzed under TEM. Golgi in differentiated keratinocytes appeared more vesiculated and dispersed. Arrowheads represent the Golgi overlap to the lysosomes. Golgi (G); lysosome (L); mitochondria (M); keratin fibers (K) and, nucleus (N). Scale bar=200 nm. (**C**) the graph is representing the % of lysosomes (L) that are closely apposed (within 150 nm) to the Golgi. Approximately 140 lysosomes from the images of multiple experiments were analyzed. (**D**) The distance (nm) between lysosomes (L) from the closest Golgi membrane in control and differentiated cells. Dotted grey line on the graph was drawn on 50nm on the X axis as a reference. The value of significance was calculated by Mann-Whitney non-parametric test. ****= $P \leq 0.0001$.

Figure 3. Generation of keratinocyte lysosomes is dependent on Golgi function. (**A**) Time lapse imaging of differentiated keratinocytes expressing Arf1^{WT}-GFP and LAMP1-RFP. Arrows and arrowheads respectively represent the localization of Arf1-GFP to the Golgi stacks and to small tubulo-vesicular structures. Time series of the white boxed region are presented. Scale bar = 5μm (in the main inset) and 2.5μm (time series). (**B**) The graph represents % of cells positive for tubulo-vesicular structures upon Arf1^{WT}-GFP expression in live and steady states. (**C**) Localization coefficients (Pearson's correlation coefficient, *r* and Mander's overlap coefficients, M1 and M2) was calculated and plotted as mean±s.e.m. ns=non-significant. (**D**) Time series imaging of differentiated keratinocytes expressing Arf1^{T31N}-GFP and LAMP1-RFP. Arrows indicate to the cytosolic localization of Arf1^{T31N}-GFP and arrowheads (in the insets) point to the punctate LAMP1 structures in the perinuclear region. Scale bar = 5μm (in the main inset) and 2.5μm (time series). (**E**) Schematic representation of Arf1 and its GEFs at *cis* and *trans*-Golgi, and their respective pharmacological inhibitors. (**F**) keratinocytes treated with respective pharmacological inhibitors were co-immunostained for GM130 and LAMP1. Insets represent 2.5 times magnification of the white boxed region. Arrowheads indicate to the Golgi with respect to lysosomes in all treatment conditions. n=number of cells. Scale bar =10 μm.

Figure 4. The peripheral Golgi protein GRASP65 surrounds the lysosomes of differentiated keratinocytes. (**A**) Live cell imaging of differentiated keratinocytes expressing GRASP65-GFP and LAMP1-RFP under Airyscan super-resolution microscope. The arrows and arrowheads represent respectively to the Golgi stacks and GRASP65-GFP ring-like structures. Scale bar =5 μm. Time series of the white-boxed region are presented. Arrowheads represent the dynamics of GRASP65-GFP ring-like structures with respect to the lysosomes. Scale bar = 2.5 μm. (**B**) The graph represents % of cells positive for GRASP65-GFP ring-like structures; n=number of cells. (**C**) The perimeter of the lysosomes (L) and, perimeter of the respective GRASP65 ring-like structures (G) was calculated; n=number of lysosomes surrounded by prominent GRASP65 ring structures (**D**-**E**) Pearson's correlation coefficient (*r)* and Mander's overlap coefficients (M1 and M2) in steady and live conditions were calculated and plotted as mean ±s.e.m.; n=number of cells. (**F**) SIM analysis of the GRASP65-GFP and LAMP1-RFP association in differentiated keratinocytes. Scale bar =1 μm. (**G**) analysis of GRASP association on the lysosomes by 3D rendering. Scale bar = 500nm. (**H-I**) The length and breadth analysis (values in nm) of lysosomes (LAMP1-RFP) and Golgi (GRASP65-GFP) were plotted as a function of fractions. 'n' in green = number of GRASP65-positive Golgi structures; 'n' in red = number of LAMP1-positive lysosome structures. (**J**) Ultrathin cryosections of differentiated keratinocytes were immunolabelled for GRASP65 (10 nm gold particles) and imaged under TEM. Arrowheads represent the localization of GRASP65 to the Golgi and lysosomes. Abbreviations are Golgi (G); lysosome (L); mitochondria (M); keratin fibers (K) and Golgi =GVs. Scale bar =200 nm. (**K**) Quantification of the % distribution of GRASP65 immunogold beads in Golgi and lysosomes. Quantification was performed including images of two independent experiments.

Figure 5. GRASP65 mediates Golgi-lysosome contacts in differentiated keratinocytes. (**A**) IFM analysis of siControl and siGRASP65 treated differentiated keratinocytes co-immunostained for GM130 and LAMP1. Cells were imaged under Airyscan super resolution microscope. Insets represent 2.5 times magnified white boxed regions. Arrows indicating to the lysosome morphology in siControl and siGRASP65 cells. Arrowheads represent the tubular LAMP1 positive structures in siGRASP65 cells. Scale bars= 10μm (main inset) and 2.5 μm (magnified inset) respectively (**B)** IFM analysis of siControl, siGRASP55, and siGRASP65 cells stained for GM130 and LAMP1. White arrows indicate the loss of Golgi-

lysosome apposition in siGRASP65 cells but not in siControl and siGRASP55 cells. (**C**) The distance between lysosome (L) and the closest Golgi stack (G) in respective siRNA treated cells was measured by using Fiji software. The distribution of the values representing G-L distance was plotted as a function of fractions. The value of significance was calculated by Kolmogorov-Smirnov non-parametric analysis. (**D**) Brief characterization of the giant LAMP1-positive structures in siGRASP65 differentiated keratinocytes. Cells were co-stained for LAMP1with either CD63, Arl8B or with internalized dextran (1st, 2nd and 4th panel). Uptake of the lysosome substrate NBD-glucosylceramide (GC) and the LysoTracker Red (the 3rd panel). Represented insets are magnified regions of the cells shown in Figure S5F. Arrows represent to the characteristics of the giant LAMP1 positive structures with respect to specific markers. Scale bar = 2.5 μm (**E**) Volumetric distribution analysis was performed as described in materials and methods. The log10 values were plotted as cumulative fractions. Statistical significance of the volume of Golgi and lysosomes in siControl or siGRASP65 cells were calculated by Mann-Whitney non parametric test.

Figure 6. Keratinocyte lysosomes derive from *trans*-Golgi. (**A**) Live cell analysis of differentiated keratinocytes expressing galT-RFP and LAMP1-GFP. Imaging was performed under Airyscan super-resolution microscope. Arrows indicate to the Golgi localized galT and arrowheads indicate the presence of galT in the lumen of lysosomes. Scale bar =5μm. (**B**) Ultrathin cryosections of differentiated keratinocytes were co-immunolabelled for galT (15 nm) and LAMP1 (10 nm). Black arrowheads represent the presence of galT in the Golgi and lysosome. G =Golgi; GVs =Golgi vesicles and L =lysosome. Scale bar =200 nm. (**C**) Quantification of the % of galT immunogold on the lysosomes and Golgi. The average percentage of the distribution of galT immunogold was calculated from three independent imaging experiments. (**D-E**) localization of the *trans* Golgi cargo and secretory cargo NPY-venus and VSVG-GFP in differentiated (D) and in control keratinocytes (E). cells were co-expressed with indicated constructs and live cell imaging was performed under a spinning disk microscope. White boxed region in the merged panel was magnified 2.5 times. Scale bars = 10μm (**F**) The model represents the generation of lysosomes from the *trans*-Golgi in differentiated keratinocytes, followed by their maturation upon receiving lysosomal and Golgi cargoes mediated by GRASP65.

Supplementary Figures:

Figure S1. Comparative analyses of the lysosomes of control and differentiated keratinocytes. (**A**) Time-lapse imaging of differentiated keratinocyte expressing LAMP1-RFP under Airyscan super-resolution microscope. Arrowheads following the dynamics of small LAMP1 carriers. Two different events from the same cell are presented (top and bottom panel). Scale bar =2.5 μm. (**B-C**) IFM analysis of control and differentiated keratinocytes co-immunostained for LAMP1 with either LAMP2 (B) or LysoTracker Red (C). Cells were visualized under Airyscan super-resolution microscope. Insets represent 2.5 times magnified white boxed regions. Arrowheads point to the colocalization between the markers. White stars represent the LAMP1 structures that are negative for LysoTracker Red. Scale bar =10 μm.

Figure S2. Presence of Golgi lysosome apposition in differentiated keratinocytes (**A**) IFM analysis of control and differentiated keratinocytes co-stained for GM130 and p230 (first panel); or LAMP1 with either GM130, p230, TGN46 or expressed Arf1-GFP. Cells were visualized under Airyscan super-resolution microscope. The numbers (1-3) on the differentiated keratinocytes represent the magnified regions presented in Fig. 2A. Insets represent 2.5 times magnified white boxed region. Pearson's correlation coefficient (*r*) and

Mander's overlap coefficients (M1 and M2) in control cells were calculated and plotted as mean±s.e.m. **** on the graphs indicates significant difference between M1 and M2 values. n= number of cells used in the quantification method. Scale bar =10 μm. (**B-C**) Comparative Golgi morphology in control and differentiated keratinocytes. Scale bars =200 nm (B). Representation of the keratinocyte lysosome morphology (in control and differentiated keratinocytes) validated by LAMP1-immunogold labelling of ultrathin cryosections. Scale bar =200 nm (C). (**D**) Control and differentiated keratinocytes were stained for WGA-alexa flour 594 and LAMP1, and visualized under Airyscan super-resolution microscope. Insets represent 2.5 times magnified white boxed region. Scale bar =10 μm. (**E**) Control and differentiated keratinocytes were co-immuno stained for LAMP1 with either LAMP2 (red=control; blue= differentiated) or DAPI respectively. The localization coefficients (Pearson's correlation coefficient (*r*) and Mander's overlap coefficients, (M1 and M2) values were plotted as mean±s.e.m. n= the number of cells used for quantifications.

Figure S3. Functional Golgi is essential for the generation of keratinocyte lysosomes. (**A**) Time lapse analysis of control keratinocytes expressing Arf1^{WT}-GFP and LAMP1-RFP. Live cell imaging was performed under Airyscan super-resolution microscope. (**B**) localization Coefficients (Pearson's correlation coefficient, *r* and Mander's overlap coefficients, M1 and M2) in control cells between Arf1-GFP and LAMP1-GFP were calculated and, plotted as mean±s.e.m. (**C**) IFM analysis of Golgi morphology of differentiated keratinocytes expressing Arf1^{T31N}-GFP, immuno stained either for GM130 or GRASP65. (**D**) analysis of lysosome morphology of control keratinocyte co-expressed with Arf1^{T31N}-GFP and LAMP1-RFP. (**E**) Control keratinocytes were treated with pharmacological inhibitors as described in materials and methods. Cells were fixed and stained for GM130 and LAMP1. Insets represent 2.5 times magnified white boxed regions. Arrows indicate to the Golgi and lysosome morphology in all treatment conditions. (**F**) Control and differentiated keratinocytes either treated with DMSO or BFA, fixed and stained for WGA alexa flour 594 (WGA-A594) and LAMP1. Insets represent 2.5 times magnified white boxed regions. Arrows indicate to the effect of BFA on the plasma membrane binding of WGA. In all images: scale bars =10 μm.

Figure S4. GRASP65 surrounds the lysosomes in differentiated keratinocytes. (**A**) Differentiated keratinocytes expressing GRASP65-GFP and GRASP55-mCherry were imaged under spinning disk microscope. Arrows and arrowheads represent respectively to the colocalization of GRASP65 with GRASP55 in dissociated Golgi stacks and, unique ring like structures of GRASP65 that are negative for GRASP55. Insets represent 2.5 times magnified white boxed regions. Scale bar = 10μm. (**B**) Live cell imaging of control keratinocytes expressing GRASP65-GFP and LAMP1-RFP under Airyscan super-resolution microscope. Scale bar =10 μm. (**C**) The graph represents % of control cells having at least one GRASP65-GFP ring in live or in steady state. (**D**-**E**) Quantification of coefficients (Pearson's correlation coefficient, *r* and Mander's overlap coefficients, M1 and M2) between GRASP65-GFP and LAMP1-RFP in the control keratinocytes in steady (D) and, in live (E) conditions. The values were plotted as mean±s.e.m. (**F**-**G**) IFM analysis of control and differentiated keratinocytes stained for LAMP1 and LC3-II (F) or endogenous GRASP65 (G). Arrowheads in (F)represent to the LC3-positive autophagosomes. Cells were imaged under Airyscan super-resolution microscope. Insets represent 2.5 times magnified white boxed regions. Scale bars =10 μm.

Figure S5. GRASP65 mediates Golgi-lysosome contacts in differentiated keratinocytes. (**A**-**C**) IFM analysis of the respective siRNA treated differentiated keratinocytes (as labelled). Cells were co immunostained for LAMP1 with either GRASP55 (A), or GRASP65 (B), or

GM130 (C) and imaged under Airyscan super resolution microscope. Insets represent 2.5 times magnified white boxed regions. Scale bar =10 μm. (**D**) Transcript analysis of GRASP65 and 55 in respective siRNA treated condition, plotted as fold change. Values of 3 independent experiments were included. (**E**) Immunoblotting analysis of control and GRASP65 knockdown cells. Blots were probed with GRAPS65 or GAPDH (as internal control). *, represents the non-specific bands. (**F)** Characterization of the giant LAMP1-positive structures in siGRASP65 differentiated keratinocytes. Cells were stained for LAMP1 and CD63 or Arl8B or internalized dextran-fluorescein (1st, 2nd and 4th panel respectively). In the 3rd panel, cells were incubated with NBD-glucosylceramide (GC) and lysotracker. White boxed regions of respective cells are magnified 2.5 times and presented in Fig. 5B. Scale bar =10 μm.

Figure S6. ManII positive Golgi structures are closely apposed to the lysosomes. (**A**) IFM analysis of differentiated keratinocytes expressing ManII-GFP and LAMP1-RFP. Cells were imaged under Airyscan super-resolution microscope. Insets from two different regions (white boxes) were magnified into 2.5 times and shown separately. Scale bar=10 μm.

Supplementary Videos:

Video S1: Live cell imaging of differentiated keratinocytes expressing LAMP1-RFP. The scale bar and time frames are mentioned in the video.

Video S2: Live cell imaging of differentiated keratinocytes expressing Arf1-GFP and LAMP1-RFP. The scale bar and time frames are mentioned in the video.

Video S3: Live cell imaging of control keratinocytes expressing Arf1-GFP and LAMP1-RFP expressed. The scale bar and time frames are mentioned in the video.

Video S4: Live cell imaging of differentiated keratinocytes expressing GRASP65-GFP and LAMP1-RFP. The scale bar and time frames are mentioned in the video.

Video S5: Live cell imaging of control keratinocytes expressing GRASP65-GFP and LAMP1-RFP expressed. The scale bar and time frames are mentioned in the video.

Author contributions:

S.M. and S.R.G.S. designed research. S.M. performed all the experiments (unless specified), analysed data and wrote the manuscript. P.B. performed electron microscopy experiments. V.B., L.E. and D.N. performed super resolution microscopy and data analysis. N.G. performed immunoblot experiments, immunofluorescence data quantification and provided technical help. G.R. and D.N. gave critical inputs during manuscript preparation. S.R.G.S and G.R. edited the manuscript. All the authors read and approved the final version of the manuscript.

Acknowledgement:

We are grateful to Satyajit Mayor (NCBS), Yanzhuang Wang (University of Michigan), Bruno Goud (Inst. Curie, Paris, France), Franck Perez (Inst. Curie, Paris, France), Nagaraj Balasubramanian (IISER Pune, India) and Amitabha Majumdar (HUL, Bangalore, India) for generous gifts of constructs and reagents. We thank Sarit Agasti, JNCASR for allowing us access Structured Illumination Microscope. Insightful discussions with Cedric Delevoye and Bruno Goud are greatly acknowledged. Kavya Gopal is acknowledged for technical help during the study.

We sincerely acknowledge IISc divisional imaging facility. We acknowledge the Nikon Imaging Center @ Institut Curie-CNRS and the PICT-IBiSA. EM sample preparation and cryosectioning at structure and membrane compartments, UMR144, Institute Curie is greatly acknowledged. We acknowledge Adrien Candat and the IBENS electron

imaging facility (IMACHEM-IBiSA), member of the French National Research infrastructure France-BioImaging.

Funding:
This work is supported by the DBT-Wellcome Trust India Alliance ECF (IA/E/17/503685) to S.M. SRGS acknowledges Science and Engineering Research Board (CRG/2019/000281), Department of Biotechnology (BT/PR4982/AGR/36/718/2012 and BT/PR32489/BRB/10/1786/2019), DBT-NBACD (BT/HRD-NBA-NWB/38/2019-20).

Conflict of interest:
The authors declare that they have no conflict of interest.

ORCIDs:
Sarmistha Mahanty: https://orcid.org/0000-0002-1111-8827

Subba Rao Gangi Setty https://orcid.org/0000-0003-4035-2900

References

Akinduro, O., K. Sully, A. Patel, D.J. Robinson, A. Chikh, G. McPhail, K.M. Braun, M.P. Philpott, C.A. Harwood, C. Byrne, R.F.L. O'Shaughnessy, and D. Bergamaschi. 2016. Constitutive Autophagy and Nucleophagy during Epidermal Differentiation. *J Invest Dermatol*. 136:1460-1470.

Atakpa, P., N.B. Thillaiappan, S. Mataragka, D.L. Prole, and C.W. Taylor. 2018. IP3 Receptors Preferentially Associate with ER-Lysosome Contact Sites and Selectively Deliver Ca(2+) to Lysosomes. *Cell Rep*. 25:3180-3193 e3187.

Ayala, I., F. Mascanzoni, and A. Colanzi. 2020. The Golgi ribbon: mechanisms of maintenance and disassembly during the cell cycle. *Biochem Soc Trans*. 48:245-256.

Ballabio, A., and J.S. Bonifacino. 2020. Lysosomes as dynamic regulators of cell and organismal homeostasis. *Nat Rev Mol Cell Biol*. 21:101-118.

Barral, D.C., L. Staiano, C. Guimas Almeida, D.F. Cutler, E.R. Eden, C.E. Futter, A. Galione, A.R.A. Marques, D.L. Medina, G. Napolitano, C. Settembre, O.V. Vieira, J. Aerts, P. Atakpa-Adaji, G. Bruno, A. Capuozzo, E. De Leonibus, C. Di Malta, C. Escrevente, A. Esposito, P. Grumati, M.J. Hall, R.O. Teodoro, S.S. Lopes, J.P. Luzio, J. Monfregola, S. Montefusco, F.M. Platt, R. Polishchuck, M. De Risi, I. Sambri, C. Soldati, and M.C. Seabra. 2022. Current methods to analyze lysosome morphology, positioning, motility and function. *Traffic*. 23:238-269.

Bikle, D.D., Z. Xie, and C.L. Tu. 2012. Calcium regulation of keratinocyte differentiation. *Expert Rev Endocrinol Metab*. 7:461-472.

Bochenska, K., M. Moskot, M. Malinowska, J. Jakobkiewicz-Banecka, A. Szczerkowska-Dobosz, D. Purzycka-Bohdan, J. Plenkowska, B. Slominski, and M. Gabig-Ciminska. 2019. Lysosome Alterations in the Human Epithelial Cell Line HaCaT and Skin Specimens: Relevance to Psoriasis. *Int J Mol Sci*. 20.

Boyce, S.T. 1994. Epidermis as a secretory tissue. *J Invest Dermatol*. 102:8-10.

Bravo-Sagua, R., N. Torrealba, F. Paredes, P.E. Morales, C. Pennanen, C. Lopez-Crisosto, R. Troncoso, A. Criollo, M. Chiong, J.A. Hill, T. Simmen, A.F. Quest, and S. Lavandero. 2014. Organelle communication: signaling crossroads between homeostasis and disease. *Int J Biochem Cell Biol*. 50:55-59.

Bright, N.A., L.J. Davis, and J.P. Luzio. 2016. Endolysosomes Are the Principal Intracellular Sites of Acid Hydrolase Activity. *Curr Biol*. 26:2233-2245.

Chu, B.B., Y.C. Liao, W. Qi, C. Xie, X. Du, J. Wang, H. Yang, H.H. Miao, B.L. Li, and B.L. Song. 2015. Cholesterol transport through lysosome-peroxisome membrane contacts. *Cell*. 161:291-306.

Colanzi, A., and D. Corda. 2007. Mitosis controls the Golgi and the Golgi controls mitosis. *Curr Opin Cell Biol*. 19:386-393.

David, Y., I.G. Castro, and M. Schuldiner. 2021. The Fast and the Furious: Golgi Contact Sites. *Contact (Thousand Oaks)*. 4:1-15.

Delevoye, C., M.S. Marks, and G. Raposo. 2019. Lysosome-related organelles as functional adaptations of the endolysosomal system. *Curr Opin Cell Biol*. 59:147-158.

Donaldson, J.G., A. Honda, and R. Weigert. 2005. Multiple activities for Arf1 at the Golgi complex. *Biochimica et Biophysica Acta (BBA) - Molecular Cell Research*. 1744:364-373.

Garcia-Mata, R., T. Szul, C. Alvarez, and E. Sztul. 2003. ADP-ribosylation factor/COPI-dependent events at the endoplasmic reticulum-Golgi interface are regulated by the guanine nucleotide exchange factor GBF1. *Mol Biol Cell*. 14:2250-2261.

Giuliani, F., A. Grieve, and C. Rabouille. 2011. Unconventional secretion: a stress on GRASP. *Curr Opin Cell Biol*. 23:498-504.

Gotz, T.W.B., D. Puchkov, V. Lysiuk, J. Lutzkendorf, A.G. Nikonenko, C. Quentin, M. Lehmann, S.J. Sigrist, and A.G. Petzoldt. 2021. Rab2 regulates presynaptic precursor vesicle biogenesis at the trans-Golgi. *J Cell Biol*. 220.

Grigoriev, I., D. Splinter, N. Keijzer, P.S. Wulf, J. Demmers, T. Ohtsuka, M. Modesti, I.V. Maly, F. Grosveld, C.C. Hoogenraad, and A. Akhmanova. 2007. Rab6 regulates transport and targeting of exocytotic carriers. *Dev Cell*. 13:305-314.

Hanus, C., and M.D. Ehlers. 2008. Secretory outposts for the local processing of membrane cargo in neuronal dendrites. *Traffic*. 9:1437-1445.

Hennings, H., F.H. Kruszewski, S.H. Yuspa, and R.W. Tucker. 1989. Intracellular calcium alterations in response to increased external calcium in normal and neoplastic keratinocytes. *Carcinogenesis*. 10:777-780.

Hurbain, I., M. Romao, P. Bergam, X. Heiligenstein, and G. Raposo. 2017. Analyzing Lysosome-Related Organelles by Electron Microscopy. *Methods Mol Biol*. 1594:43-71.

Ireland, S., S. Ramnarayanan, M. Fu, X. Zhang, J. Zhang, J. Li, D. Emebo, and Y. Wang. 2020. Cytosolic Ca(2+) Modulates Golgi Structure Through PKCalpha-Mediated GRASP55 Phosphorylation. *iScience*. 23:100952.

Ishizaki, R., H.W. Shin, H. Mitsuhashi, and K. Nakayama. 2008. Redundant roles of BIG2 and BIG1, guanine-nucleotide exchange factors for ADP-ribosylation factors in membrane traffic between the trans-Golgi network and endosomes. *Mol Biol Cell*. 19:2650-2660.

Katz, A.B., and L.B. Taichman. 1994. Epidermis as a secretory tissue: an in vitro tissue model to study keratinocyte secretion. *J Invest Dermatol*. 102:55-60.

Kawamoto, K., Y. Yoshida, H. Tamaki, S. Torii, C. Shinotsuka, S. Yamashina, and K. Nakayama. 2002. GBF1, a guanine nucleotide exchange factor for ADP-ribosylation factors, is localized to the cis-Golgi and involved in membrane association of the COPI coat. *Traffic*. 3:483-495.

Khatter, D., V.B. Raina, D. Dwivedi, A. Sindhwani, S. Bahl, and M. Sharma. 2015. The small GTPase Arl8b regulates assembly of the mammalian HOPS complex on lysosomes. *J Cell Sci*. 128:1746-1761.

Kornfeld, S., and I. Mellman. 1989. The biogenesis of lysosomes. *Annu Rev Cell Biol*. 5:483-525.

Krause, W.J. 2000. Brunner's glands: a structural, histochemical and pathological profile. *Prog Histochem Cytochem*. 35:259-367.

Kreft, M.E., A.A. Mironov, and S. Hudoklin. 2022. The Golgi complex: An organelle that determines urothelial cell biology in health and disease. *Histochem Cell Biol*. 158:229-240.

Kumari, S., and S. Mayor. 2008. ARF1 is directly involved in dynamin-independent endocytosis. *Nat Cell Biol*. 10:30-41.

Lie, P.P.Y., D.S. Yang, P. Stavrides, C.N. Goulbourne, P. Zheng, P.S. Mohan, A.M. Cataldo, and R.A. Nixon. 2021. Post-Golgi carriers, not lysosomes, confer lysosomal properties to pre-degradative organelles in normal and dystrophic axons. *Cell Rep*. 35:109034.

Mahanty, S., S.S. Dakappa, R. Shariff, S. Patel, M.M. Swamy, A. Majumdar, and S.R.G. Setty. 2019. Keratinocyte differentiation promotes ER stress-dependent lysosome biogenesis. *Cell Death Dis*. 10:269.

Mahanty, S., and S.R.G. Setty. 2021. Epidermal Lamellar Body Biogenesis: Insight Into the Roles of Golgi and Lysosomes. *Front Cell Dev Biol*. 9:701950.

Makhoul, C., and P.A. Gleeson. 2021. Regulation of mTORC1 activity by the Golgi apparatus. *Fac Rev*. 10:50.

Manolea, F., A. Claude, J. Chun, J. Rosas, and P. Melancon. 2008. Distinct functions for Arf guanine nucleotide exchange factors at the Golgi complex: GBF1 and BIGs are required for assembly and maintenance of the Golgi stack and trans-Golgi network, respectively. *Mol Biol Cell*. 19:523-535.

Marra, P., T. Maffucci, T. Daniele, G.D. Tullio, Y. Ikehara, E.K. Chan, A. Luini, G. Beznoussenko, A. Mironov, and M.A. De Matteis. 2001. The GM130 and GRASP65 Golgi proteins cycle through and define a subdomain of the intermediate compartment. *Nat Cell Biol*. 3:1101-1113.

Marwaha, R., S.B. Arya, D. Jagga, H. Kaur, A. Tuli, and M. Sharma. 2017. The Rab7 effector PLEKHM1 binds Arl8b to promote cargo traffic to lysosomes. *J Cell Biol*. 216:1051-1070.

Monteleon, C.L., T. Agnihotri, A. Dahal, M. Liu, V.W. Rebecca, G.L. Beatty, R.K. Amaravadi, and T.W. Ridky. 2018. Lysosomes Support the Degradation, Signaling, and Mitochondrial Metabolism Necessary for Human Epidermal Differentiation. *J Invest Dermatol*. 138:1945-1954.

Murphy, R.F. 1991. Maturation models for endosome and lysosome biogenesis. *Trends Cell Biol*. 1:77-82.

Nebenfuhr, A., C. Ritzenthaler, and D.G. Robinson. 2002. Brefeldin A: deciphering an enigmatic inhibitor of secretion. *Plant Physiol*. 130:1102-1108.

Nickel, W. 2010. Pathways of unconventional protein secretion. *Curr Opin Biotechnol*. 21:621-626.

Patwardhan, A., S. Bardin, S. Miserey-Lenkei, L. Larue, B. Goud, G. Raposo, and C. Delevoye. 2017. Routing of the RAB6 secretory pathway towards the lysosome related organelle of melanocytes. *Nat Commun*. 8:15835.

Pols, M.S., E. van Meel, V. Oorschot, C. ten Brink, M. Fukuda, M.G. Swetha, S. Mayor, and J. Klumperman. 2013. hVps41 and VAMP7 function in direct TGN to late endosome transport of lysosomal membrane proteins. *Nat Commun*. 4:1361.

Presley, J.F., C. Smith, K. Hirschberg, C. Miller, N.B. Cole, K.J. Zaal, and J. Lippincott-Schwartz. 1998. Golgi membrane dynamics. *Mol Biol Cell*. 9:1617-1626.

Rabouille, C., and A.D. Linstedt. 2016. GRASP: A Multitasking Tether. *Front Cell Dev Biol*. 4:1.

Rambourg, A., Y. Clermont, M. Chretien, and L. Olivier. 1993. Modulation of the Golgi apparatus in stimulated and nonstimulated prolactin cells of female rats. *Anat Rec*. 235:353-362.

Satoh, A., Y. Hasegawa, and Y. Honjo. 2015. The Roles of GRASP55/65 in Golgi Formation and Function. *Trends in Glycoscience and Glycotechnology*. 27:33-36.

Schaub, B.E., B. Berger, E.G. Berger, and J. Rohrer. 2006. Transition of galactosyltransferase 1 from trans-Golgi cisterna to the trans-Golgi network is signal mediated. *Mol Biol Cell*. 17:5153-5162.

Scott, K.L., O. Kabbarah, M.C. Liang, E. Ivanova, V. Anagnostou, J. Wu, S. Dhakal, M. Wu, S. Chen, T. Feinberg, J. Huang, A. Saci, H.R. Widlund, D.E. Fisher, Y. Xiao, D.L. Rimm, A. Protopopov, K.K. Wong, and L. Chin. 2009. GOLPH3 modulates mTOR signalling and rapamycin sensitivity in cancer. *Nature*. 459:1085-1090.

Singh, V., C. Erady, and N. Balasubramanian. 2018. Cell-matrix adhesion controls Golgi organization and function through Arf1 activation in anchorage-dependent cells. *J Cell Sci*. 131.

Spang, A. 2002. ARF1 regulatory factors and COPI vesicle formation. *Curr Opin Cell Biol*. 14:423-427.

Starling, G.P., Y.Y. Yip, A. Sanger, P.E. Morton, E.R. Eden, and M.P. Dodding. 2016. Folliculin directs the formation of a Rab34-RILP complex to control the nutrient-dependent dynamic distribution of lysosomes. *EMBO Rep*. 17:823-841.

Thayer, D.A., Y.N. Jan, and L.Y. Jan. 2013. Increased neuronal activity fragments the Golgi complex. *Proc Natl Acad Sci U S A*. 110:1482-1487.

Thomas, J.D., Y.J. Zhang, Y.H. Wei, J.H. Cho, L.E. Morris, H.Y. Wang, and X.F. Zheng. 2014. Rab1A is an mTORC1 activator and a colorectal oncogene. *Cancer Cell*. 26:754-769.

Venkatachalapathy, M., V. Belapurkar, M. Jose, A. Gautier, and D. Nair. 2019. Live cell super resolution imaging by radial fluctuations using fluorogen binding tags. *Nanoscale*. 11:3626-3632.

Walton, K., A. Leier, and E. Sztul. 2020. Regulating the regulators: role of phosphorylation in modulating the function of the GBF1/BIG family of Sec7 ARF-GEFs. *FEBS Lett*. 594:2213-2226.

Wang, T., and W. Hong. 2002. Interorganellar regulation of lysosome positioning by the Golgi apparatus through Rab34 interaction with Rab-interacting lysosomal protein. *Mol Biol Cell*. 13:4317-4332.

Wang, Y., A. Satoh, and G. Warren. 2005. Mapping the functional domains of the Golgi stacking factor GRASP65. *J Biol Chem*. 280:4921-4928.

Wang, Y., J.H. Wei, B. Bisel, D. Tang, and J. Seemann. 2008. Golgi cisternal unstacking stimulates COPI vesicle budding and protein transport. *PLoS One*. 3:e1647.

Wei, J.H., and J. Seemann. 2017. Golgi ribbon disassembly during mitosis, differentiation and disease progression. *Curr Opin Cell Biol*. 47:43-51.

Wong, Y.C., S. Kim, W. Peng, and D. Krainc. 2019. Regulation and Function of Mitochondria-Lysosome Membrane Contact Sites in Cellular Homeostasis. *Trends Cell Biol*. 29:500-513.

Xiang, Y., and Y. Wang. 2010. GRASP55 and GRASP65 play complementary and essential roles in Golgi cisternal stacking. *J Cell Biol*. 188:237-251.

Xiang, Y., X. Zhang, D.B. Nix, T. Katoh, K. Aoki, M. Tiemeyer, and Y. Wang. 2013. Regulation of protein glycosylation and sorting by the Golgi matrix proteins GRASP55/65. *Nat Commun*. 4:1659.

Yamanishi, H., T. Soma, J. Kishimoto, T. Hibino, and A. Ishida-Yamamoto. 2019. Marked Changes in Lamellar Granule and Trans-Golgi Network Structure Occur during Epidermal Keratinocyte Differentiation. *J Invest Dermatol*. 139:352-359.

Yang, J.S., C. Valente, R.S. Polishchuk, G. Turacchio, E. Layre, D.B. Moody, C.C. Leslie, M.H. Gelb, W.J. Brown, D. Corda, A. Luini, and V.W. Hsu. 2011. COPI acts in both vesicular and tubular transport. *Nat Cell Biol*. 13:996-1003.

Yoshihara, N., T. Ueno, A. Takagi, J.A. Oliva Trejo, K. Haruna, Y. Suga, M. Komatsu, K. Tanaka, and S. Ikeda. 2015. The significant role of autophagy in the granular layer in normal skin differentiation and hair growth. *Arch Dermatol Res*. 307:159-169.

Zhang, X., L. Wang, B. Lak, J. Li, E. Jokitalo, and Y. Wang. 2018. GRASP55 Senses Glucose Deprivation through O-GlcNAcylation to Promote Autophagosome-Lysosome Fusion. *Dev Cell*. 45:245-261 e246.

Zhang, X., and Y. Wang. 2015. GRASPs in Golgi Structure and Function. *Front Cell Dev Biol*. 3:84.

Zhang, X., and Y. Wang. 2018. GRASP55 facilitates autophagosome maturation under glucose deprivation. *Mol Cell Oncol*. 5:e1494948.

Zhang, X., and Y. Wang. 2020. Nonredundant Roles of GRASP55 and GRASP65 in the Golgi Apparatus and Beyond. *Trends Biochem Sci*. 45:1065-1079.

Figure 1.

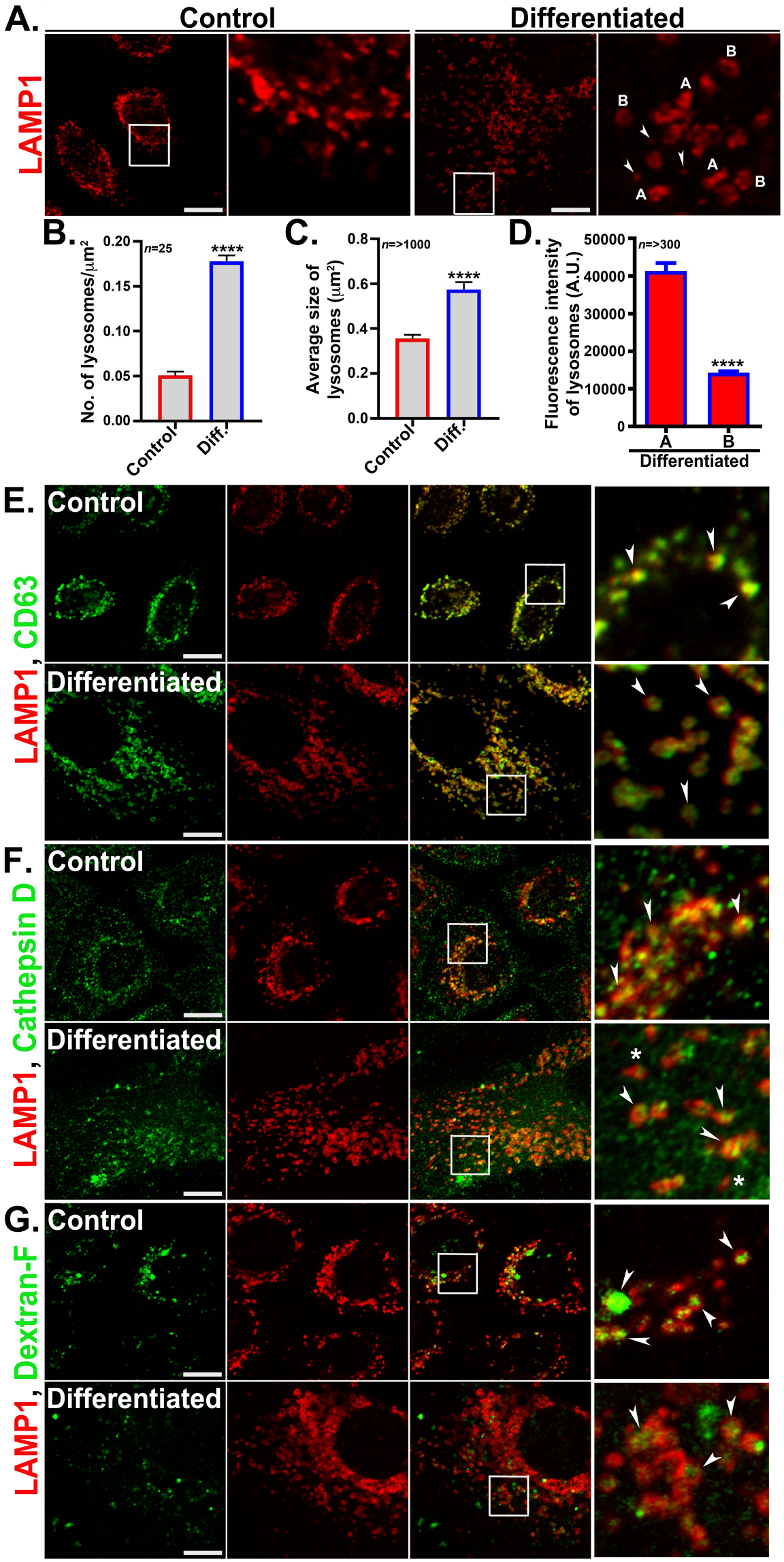
A.
Control
Differentiated
LAMP1
B
A
B
A
A
B
B.
No. of lysosomes/μm²
n=25
****
0.20
0.15
0.10
0.05
0.00
Control
Diff.
C.
Average size of lysosomes (μm²)
n=>1000
****
0.8
0.6
0.4
0.2
0.0
Control
Diff.
D.
Fluorescence intensity of lysosomes (A.U.)
n=>300
****
50000
40000
30000
20000
10000
0
A
B
Differentiated
E.
Control
Differentiated
LAMP1, CD63
F.
Control
Differentiated
LAMP1, Cathepsin D
*
*
G.
Control
Differentiated
LAMP1, Dextran-F

Figure 2.

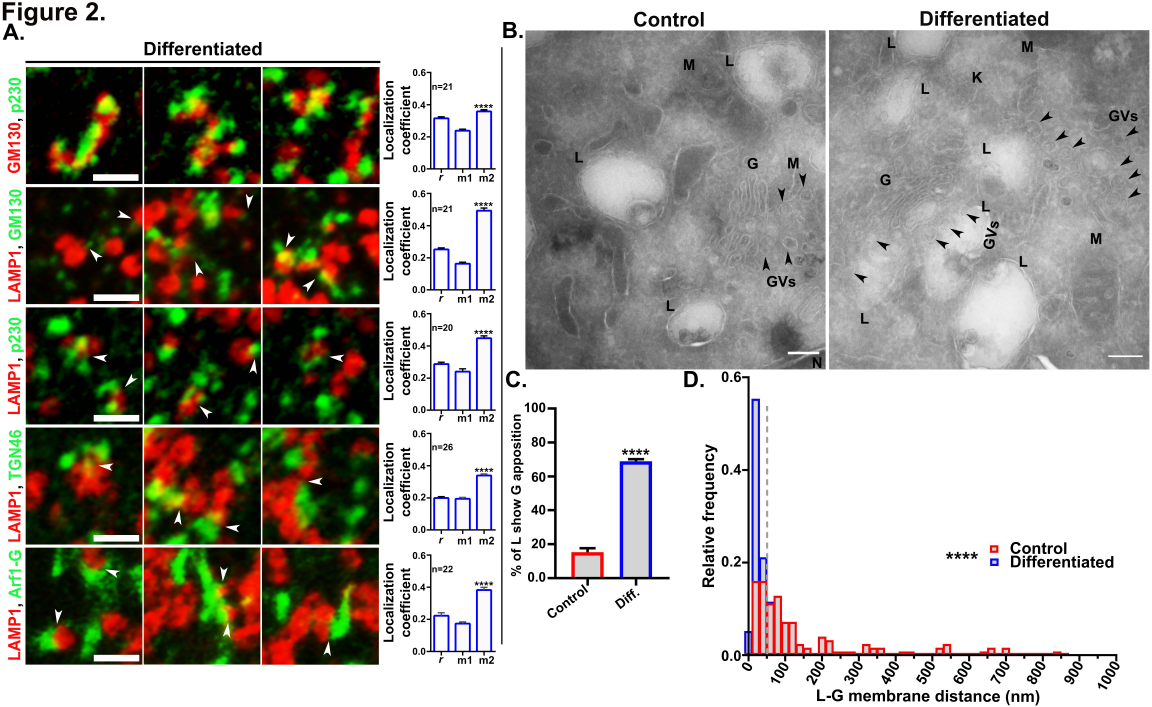
A.
Differentiated
GM130, p230
LAMP1, GM130
LAMP1, p230
LAMP1, TGN46
LAMP1, Arf1-G
Localization coefficient
n=21
n=21
n=20
n=26
n=22
****
r
m1
m2
B.
Control
Differentiated
M
L
G
GVs
K
N
C.
% of L show G apposition
Control
Diff.
D.
Relative frequency
L-G membrane distance (nm)
Control
Differentiated

Figure 3.

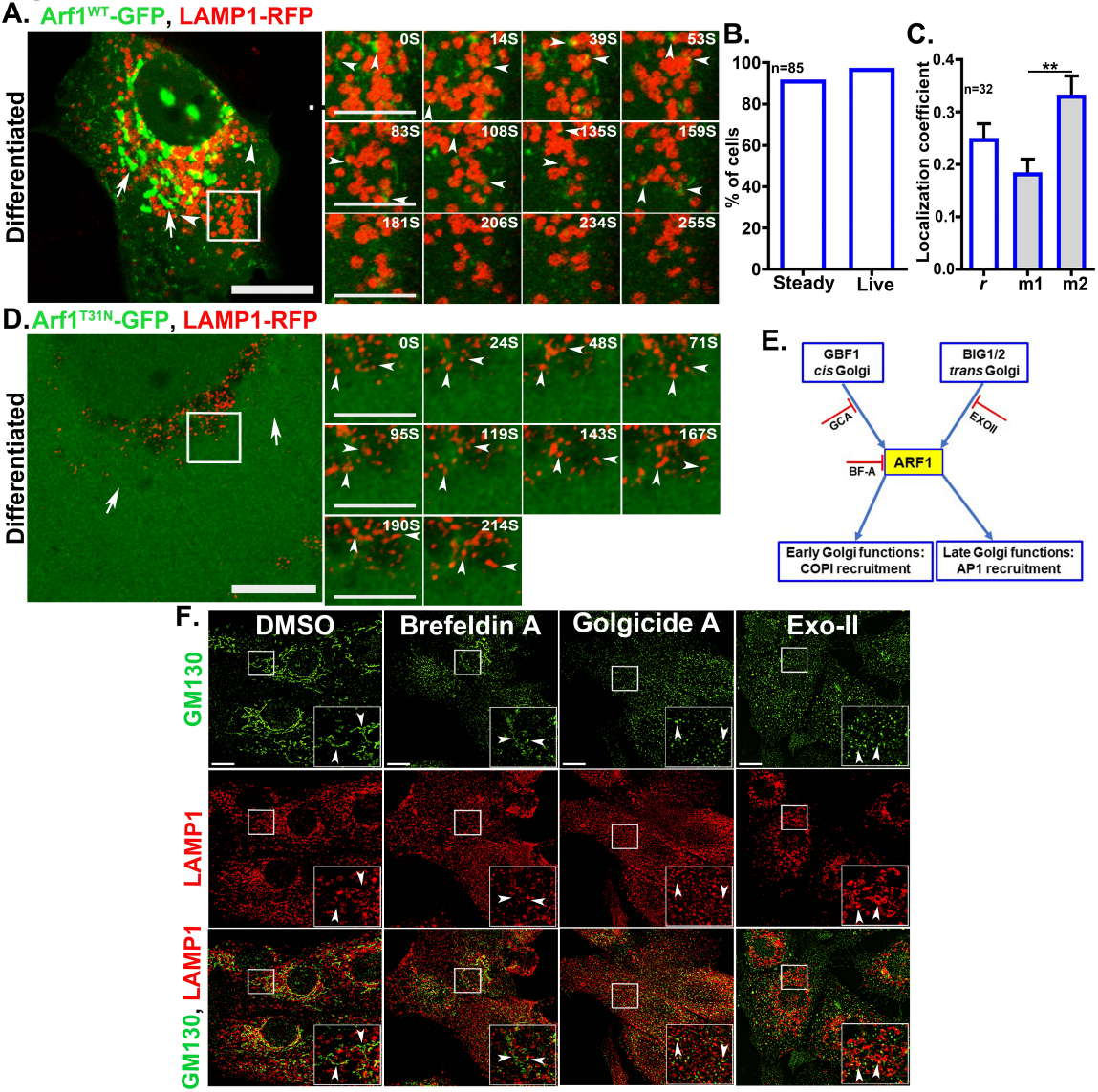
A. Arf1WT-GFP, LAMP1-RFP
Differentiated
0S
14S
39S
53S
83S
108S
135S
159S
181S
206S
234S
255S
B.
n=85
% of cells
Steady
Live
C.
n=32
**
Localization coefficient
r
m1
m2
D. Arf1T31N-GFP, LAMP1-RFP
Differentiated
0S
24S
48S
71S
95S
119S
143S
167S
190S
214S
E.
GBF1
cis Golgi
BIG1/2
trans Golgi
GCA
EXOII
BF-A
ARF1
Early Golgi functions:
COPI recruitment
Late Golgi functions:
AP1 recruitment
F.
DMSO
Brefeldin A
Golgicide A
Exo-II
GM130
LAMP1
GM130, LAMP1

Figure 4.

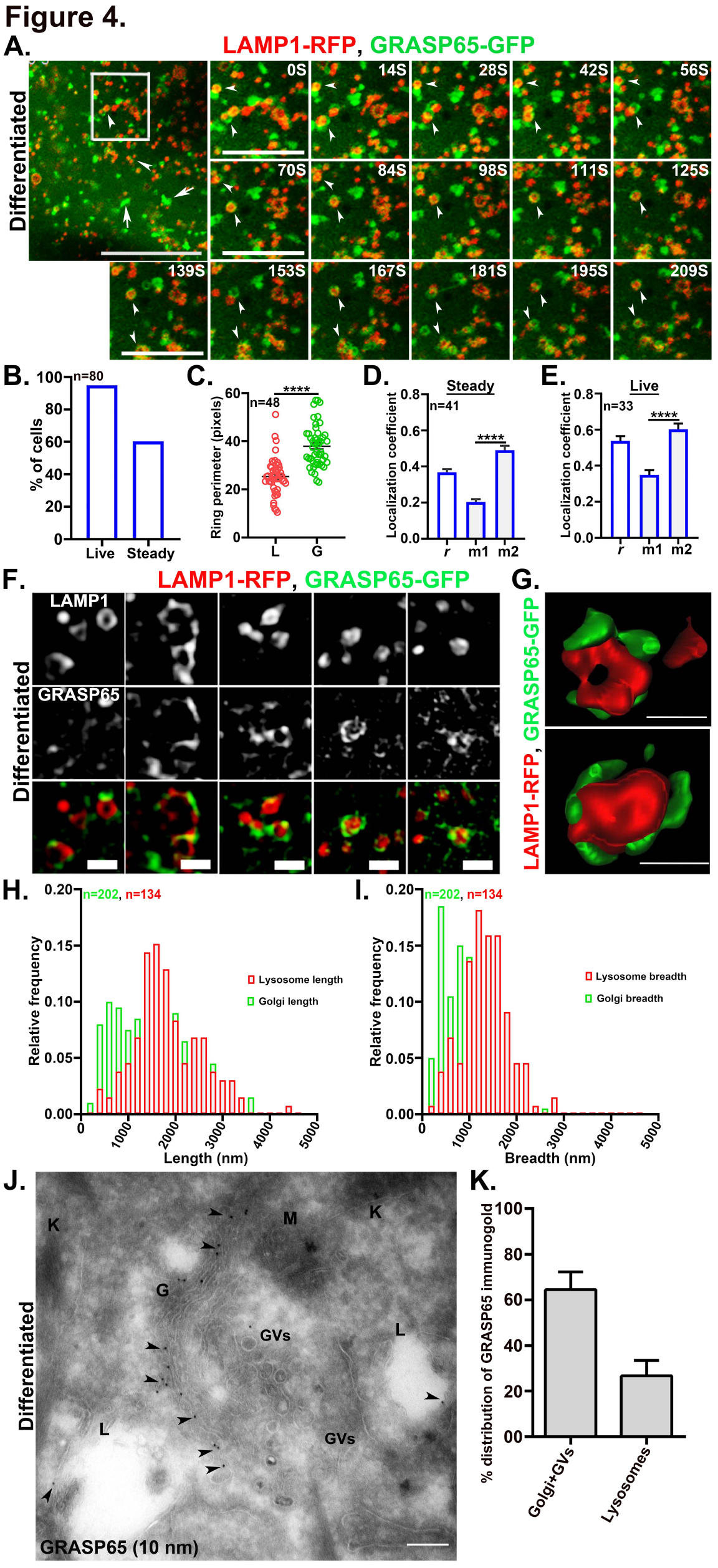
A.
LAMP1-RFP, GRASP65-GFP
Differentiated
0S
14S
28S
42S
56S
70S
84S
98S
111S
125S
139S
153S
167S
181S
195S
209S
B.
n=80
% of cells
Live
Steady
C.
n=48
****
Ring perimeter (pixels)
L
G
D.
Steady
n=41
****
Localization coefficient
r
m1
m2
E.
Live
n=33
****
Localization coefficient
r
m1
m2
F.
LAMP1-RFP, GRASP65-GFP
LAMP1
GRASP65
Differentiated
G.
LAMP1-RFP, GRASP65-GFP
H.
n=202, n=134
Relative frequency
Lysosome length
Golgi length
Length (nm)
I.
n=202, n=134
Relative frequency
Lysosome breadth
Golgi breadth
Breadth (nm)
J.
K
M
K
G
GVs
L
L
GVs
Differentiated
GRASP65 (10 nm)
K.
% distribution of GRASP65 immunogold
Golgi+GVs
Lysosomes

Figure 5.

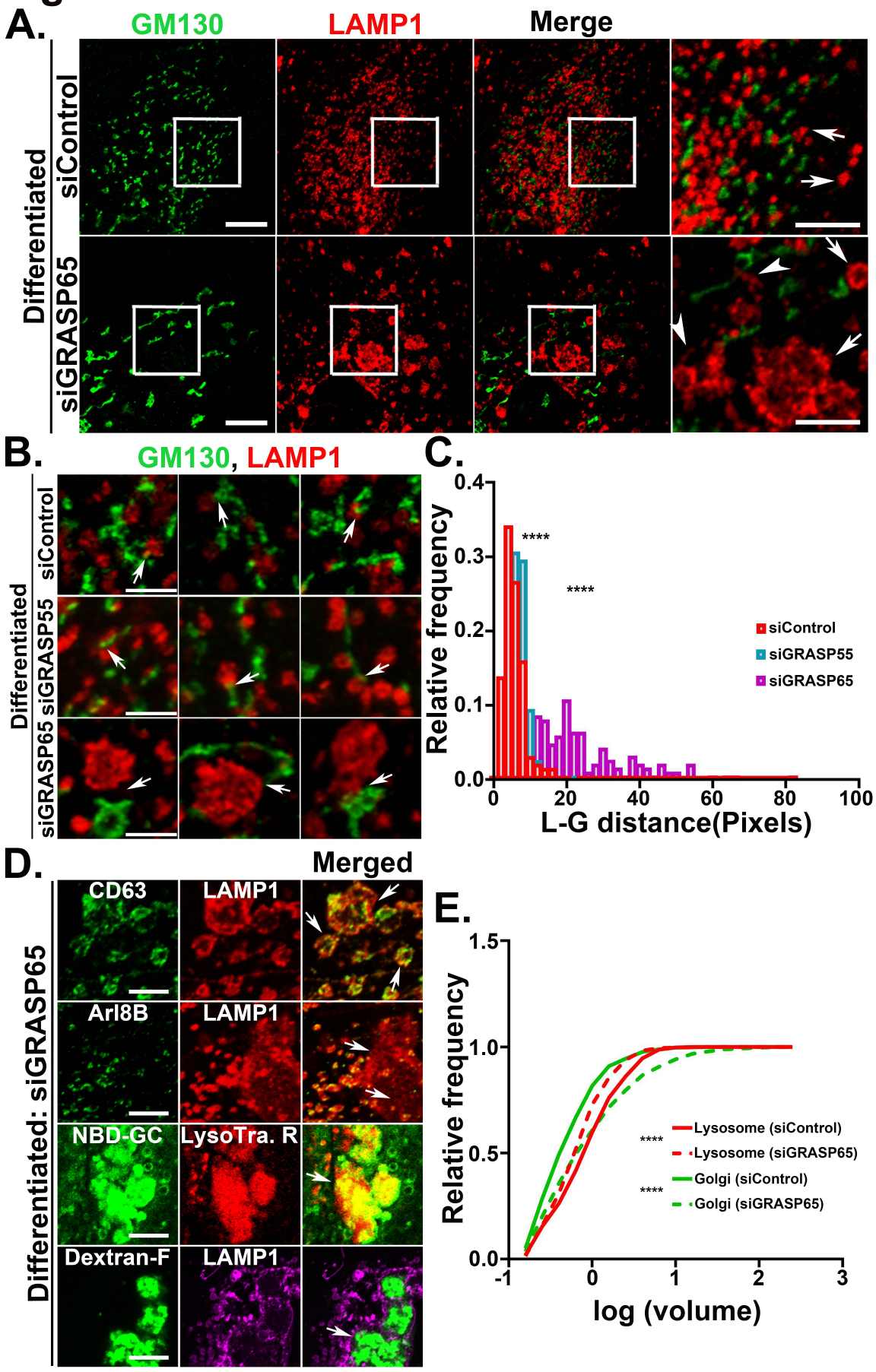
A.
GM130
LAMP1
Merge
Differentiated
siControl
siGRASP65
B.
GM130, LAMP1
Differentiated
siControl
siGRASP55
siGRASP65
C.
Relative frequency
0.4
0.3
0.2
0.1
0.0
****
****
siControl
siGRASP55
siGRASP65
0
20
40
60
80
100
L-G distance(Pixels)
D.
Merged
Differentiated: siGRASP65
CD63
LAMP1
Arl8B
LAMP1
NBD-GC
LysoTra. R
Dextran-F
LAMP1
E.
Relative frequency
1.5
1.0
0.5
0.0
****
****
Lysosome (siControl)
Lysosome (siGRASP65)
Golgi (siControl)
Golgi (siGRASP65)
-1
0
1
2
3
log (volume)

Figure 6.

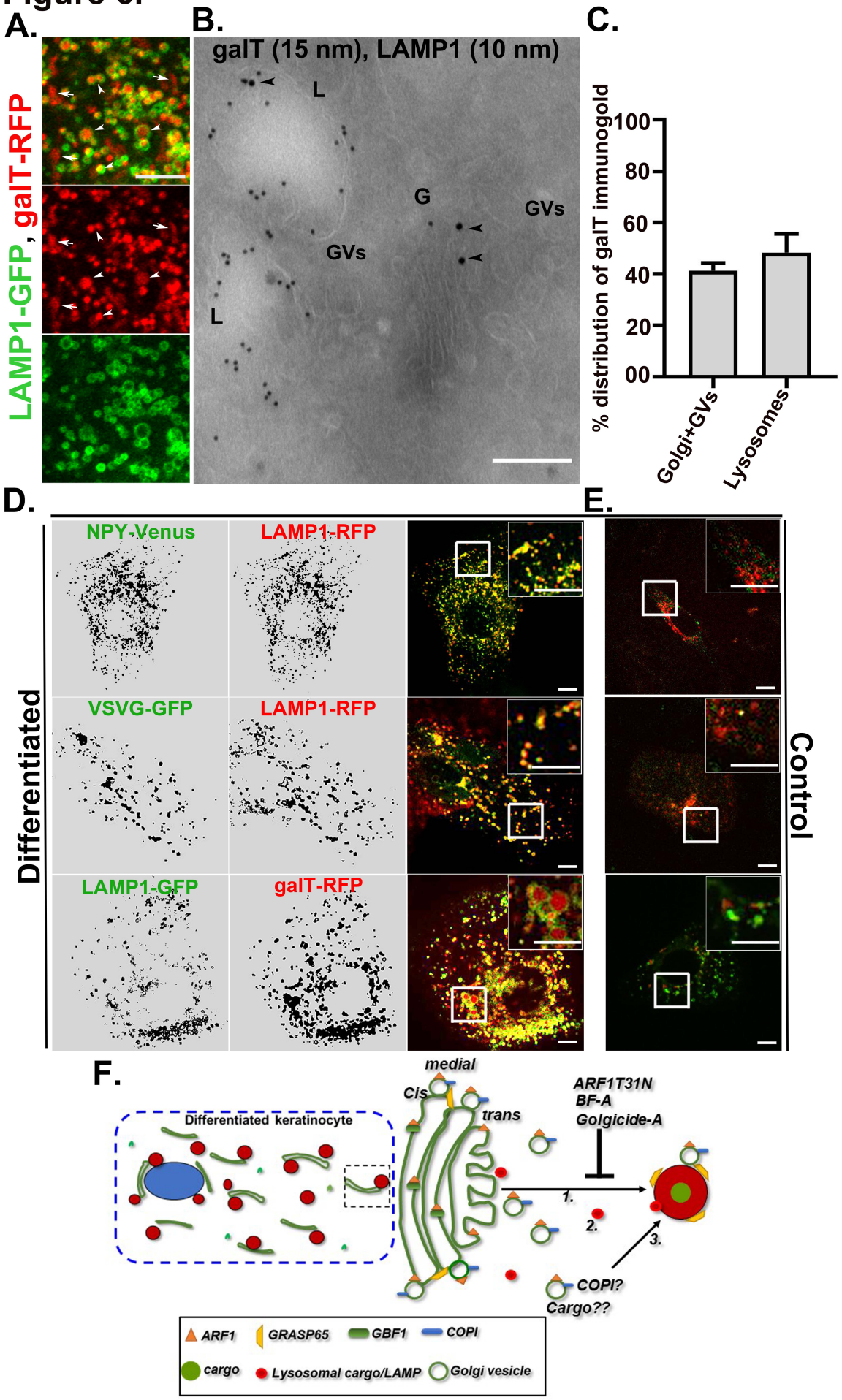
A.
LAMP1-GFP, galT-RFP
B.
galT (15 nm), LAMP1 (10 nm)
L
G
GVs
GVs
L
C.
% distribution of galT immunogold
100
80
60
40
20
00
Golgi+GVs
Lysosomes
D.
E.
NPY-Venus
LAMP1-RFP
VSVG-GFP
LAMP1-RFP
LAMP1-GFP
galT-RFP
Differentiated
Control
F.
Differentiated keratinocyte
medial
Cis
trans
ARF1T31N
BF-A
Golgicide-A
1.
2.
3.
COPI?
Cargo??
ARF1
GRASP65
GBF1
COPI
cargo
Lysosomal cargo/LAMP
Golgi vesicle